Supernova tests of the timescape cosmology

Peter R. Smale⋆ & David L. Wiltshire†

Department of Physics & Astronomy, University of Canterbury, Private Bag 4800, Christchurch 8140, New Zealand

ABSTRACT

The timescape cosmology has been proposed as a viable alternative to homogeneous cosmologies with dark energy. It realises cosmic acceleration as an apparent effect that arises in calibrating average cosmological parameters in the presence of spatial curvature and gravitational energy gradients that grow large with the growth of inhomogeneities at late epochs. Recently Kwan, Francis and Lewis have claimed that the timescape model provides a relatively poor fit to the Union and Constitution supernovae compilations, as compared to the standard ΛCDM model. We show this conclusion is a result of systematic issues in supernova light curve fitting, and of failing to exclude data below the scale of statistical homogeneity, $z \lesssim 0.033$. Using all currently available supernova datasets (Gold07, Union, Constitution, MLCS17, MLCS31, SDSS-II, CSP, Union2), and making cuts at the statistical homogeneity scale, we show that data reduced by the SALT/SALT-II fitters provides Bayesian evidence that favours the spatially flat ΛCDM model over the timescape model, whereas data reduced with MLCS2k2 fitters gives Bayesian evidence which favours the timescape model over the ΛCDM model. We discuss the questions of extinction and reddening by dust, and of intrinsic colour variations in supernovae which do not correlate with the decay time, and the likely impact these systematics would have in a scenario consistent with the timescape model.

Key words: cosmology: cosmological parameters — cosmology: observations — cosmology: theory

1 INTRODUCTION

The enigma of a late epoch apparent acceleration of the expansion of the universe is one of the greatest fundamental challenges we have ever faced in theoretical cosmology. Our standard understanding is that this is probably due to the present–day universe being dominated by a cosmological constant or other fluid–like "dark energy" with an equation of state, $P = w\rho$, which violates the strong energy condition. However, this conclusion is based on the assumption that the universe is well–described by a geometry which is exactly a homogeneous and isotropic Friedmann–Lemaître–Robertson–Walker (FLRW) model, with additional Newtonian perturbations. Observationally, however, the assumption of homogeneity is open to challenges.

At the epoch of last scattering the matter distribution was certainly very homogeneous, given the evidence of the cosmic microwave background (CMB) radiation. Furthermore, if we look back to galaxies at large redshifts early in cosmic history, such as those in the Hubble Deep Field,

then the distribution is relatively homogeneous. However, in the intervening aeons the matter distribution has become very inhomogeneous through the growth of structure. Large scale surveys reveal the present epoch universe to possess a cosmic web of structures, dominated in volume by voids, with galaxy clusters strung in sheets that surround the voids, and filaments that thread them. Surveys indicate that 40-50% of the nearby universe is in voids of a characteristic diameter of $30h^{-1}$ Mpc (Hoyle & Vogeley 2002, 2004). Once numerous additional minivoids (Tikhonov & Karachentsev 2006) are included, the present epoch universe appears to be void–dominated. Statistical homogeneity of this structure appears only to be reached by averaging on scales of order at least $100h^{-1}$ Mpc or more, where h is the dimensionless parameter related to the Hubble constant by $H_0 = 100h\,\mathrm{km}\ \mathrm{sec}^{-1}\,\mathrm{Mpc}^{-1}$. The problem of fitting a smooth geometry to a universe with such a lumpy matter distribution (Ellis 1984; Ellis & Stoeger 1984) is a nontrivial one, but central to relating observations to the numerical values of the averaged parameters which describe the Universe and its evolution as a whole.

The timescape (TS) cosmological model (Wiltshire 2007a,b, 2009) has been proposed as a potentially viable

---

⋆ E-mail: peter.smale@pg.canterbury.ac.nz
† E-mail: David.Wiltshire@canterbury.ac.nz

alternative to homogeneous cosmology with fluid-like dark energy. It begins from the premise, consistent with observations of void statistics, that the present epoch universe is strongly inhomogeneous on scales below the Baryon Acoustic Oscillation (BAO) scale of order $100h^{-1}$ Mpc, while exhibiting a variance of density of order 8% in density for sample volumes larger than this scale (Hogg et al. 2005; Sylos Labini et al. 2009). This is consistent with the growth of density contrasts with initially small fluctuations $\delta\rho/\rho \sim 10^{-4}$ in dark matter at last scattering, without assuming evolution by a single Friedmann scale factor for the whole universe (Wiltshire 2009). The reason for a $100h^{-1}$ Mpc cutoff for this "scale of statistical homogeneity" is that below this scale density contrasts at last scattering are amplified by the acoustic waves in the primordial plasma.

In the two–scale model of Wiltshire (2007a,b, 2009) cosmic evolution is determined by a Buchert average (Buchert 2000) over spatially flat wall regions, assumed to contain all gravitationally bound structures, and negatively curved voids. In the timescape scenario there is a crucial ingredient in the physical interpretation of the Buchert average, which has not been pursued in other investigations using the Buchert formalism. (See, e.g., Buchert (2008) for a recent review.) In particular, given that the Buchert average is a statistical average taken by volume, then for a universe which is void–dominated at late epochs the local geometry at a volume–average location can differ considerably from that of sources and observers in gravitationally bound systems within galaxies within the wall regions. It is hypothesised that quasi-local gravitational energy gradients result from the density and spatial curvature gradients between the two locations. In particular, a substantial difference in clock rates arises cumulatively over the lifetime of the universe from the tiny relative volume deceleration of voids as compared to wall regions (Wiltshire 2008). The magnitude of this relative deceleration, typically of order $10^{-10}\,\mathrm{m\,s^{-2}}$ over much of the lifetime of the universe, is consistent with weak–field expectations, and may be understood conceptually in terms of a generalisation of the equivalence principle (Wiltshire 2008).

The faintness of type Ia supernovae (SNe Ia) relative to the expectations of matter–dominated homogeneous cosmologies then arises both as a consequence of: (i) the changes to cosmic evolution that arise in a Buchert average of the Einstein equations; and (ii) the growing differences in the calibration of the notional clocks and rulers of an ideal volume–average observer as compared to the actual clocks and rulers of observers confined to gravitationally bound systems. In particular, cosmic acceleration is an apparent effect: a volume–average observer in a void would not infer any cosmic acceleration, but observers in galaxies do (Wiltshire 2007a). This provides a natural solution to the cosmic coincidence problem, since apparent acceleration is only registered once the void fraction reaches a critical threshold of 59%, typically near a redshift $z \sim 0.9$ (Wiltshire 2007a).

Leith, Ng & Wiltshire (2008) considered some preliminary quantitative tests of the TS model, concentrating in particular on the fit of the 182 SN Ia distance moduli in the Gold dataset of Riess et al. (2007) (Riess07). It was found that the TS model gave a relatively good fit to the Riess07 data, as compared to the spatially flat ΛCDM model. This conclusion has recently been challenged by Kwan, Francis &

Lewis (2009), who concluded that the TS model proved to be a poorer fit than the spatially flat ΛCDM model when tested with the more recent and larger Union (Kowalski et al. 2008) and Constitution (Hicken et al. 2009) SN Ia datasets. Furthermore, the best–fit value of the TS dressed matter density parameter was found by Kwan et al. (2009) to be driven to values an order of magnitude smaller than the Leith et al. (2008) fit $\Omega_{m0} = 0.33^{+0.11}_{-0.16}$.

In this paper, we reply to Kwan et al. (2009) by investigating the fit of the TS model to a number of recent SneIa datasets fit by different data reduction methods, giving careful consideration to the systematic issues that arise when one is dealing with a nonstandard cosmological model. These issues were not considered by Kwan et al. In the course of our investigations we have uncovered one error in the Leith et al. (2008) paper: on account of a bug in a numerical code the value of the Bayes factor that was quoted there was incorrect[1]. Rather than a Bayes factor, $\ln B = 0.27$ in favour of the TS model over the spatially flat ΛCDM model, the Bayes factor relative to the Riess07 data is in fact $\ln B = -1.12$ for the given priors with $0.01 \leqslant \Omega_{m0} \leqslant 0.5$. In other words, rather than being statistically indistinguishable, the Riess07 data in fact provides mild positive evidence in favour of the spatially flat ΛCDM model as compared to the TS model. This numerical error was not raised by Kwan et al. (2009), however. Rather, the main criticism[2] of Kwan et al. (2009) is a relatively poor fit of the TS model to the Union and Constitution datasets. As we will see, this conclusion relies

---

[1] This numerical error in the routine used in the Bayesian integration does not affect any other numerical results given in Leith et al. (2008).

[2] In addition to the principal discussion of fits to SneIa data, Kwan et al. (2009) also make some apparently critical remarks about the TS model which deserve some reply. Firstly, Kwan et al. comment that Birkhoff's theorem is not relevant to the TS cosmology. However, Birkhoff's theorem – namely the statement that the unique spherically symmetric solution of the *vacuum* Einstein equations is the Schwarzschild solution – is not relevant in any circumstance in which the energy–momentum tensor of matter is non-zero, which also includes the standard FLRW cosmology with a dust or perfect fluid source. This comment is therefore gratuitous. Secondly, Kwan et al. also state that the Newtonian limit is not relevant in the TS cosmology. This remark is simply incorrect, and is presumably based on incomplete reading of Wiltshire (2007a, 2008). In the absence of a simple background geometry, which is the case in a genuinely inhomogeneous background, then the correct derivation of the Newtonian limit, together with post–Newtonian corrections, is a subtle and nontrivial problem which is much more complicated than the case of the standard perturbed FLRW universe, as was discussed in Sec. 8.4 of Wiltshire (2007a). One reason for proposing an extension of the strong equivalence principle to the cosmological equivalence principle (Wiltshire 2008) is the hope that it might ultimately provide a framework for establishing a Newtonian limit in the case that there are strong inhomogeneities in the background geometry. The fact that a post–Newtonian framework has not yet been worked out in detail is simply due to the TS cosmology being work in progress. Finally, the claim that the TS model suffers a "failure to provide any predictions on cosmological parameters that are directly observable" (Kwan et al. 2009) is refuted by Wiltshire (2009), where several cosmological tests with the potential to distinguish the TS cosmology from the standard FLRW cosmology are discussed in detail.

on the naïve use of data which has been reduced assuming the standard cosmology by the SALT methods. One particularly important consideration in analysing the data is that a cut should always be made at the scale of statistical homogeneity expected in the TS model – a fact that Kwan et al. omitted. We shall see that depending on the dataset and fitting method used, in some cases the TS model provides a fit that is either statistically indistinguishable from ΛCDM, or mildly favoured or disfavoured on Bayesian evidence. However, given other unknown systematic differences between the variants of the SALT and MLCS methods, at present it is fair to say one cannot reliably distinguish the TS and ΛCDM models on the basis of SNe Ia data alone.

The outline of the paper is as follows. In section 2 we give a brief overview of the timescape cosmology, while in section 3 we given an overview of the SN Ia light curve data reduction methods. In section 4 we analyse the currently available data, considering in particular the issues of recalibrating the SALT light curve fitter, exclusion of data below the statistical homogeneity scale, and differences between the various SNe Ia datasets. In section 5 we discuss the impact that unknown systematic issues, particularly concerning intrinsic colours variations and reddening and extinction, may have on the comparison of the TS with the standard cosmology.

2   THE TIMESCAPE MODEL

In keeping with current observations that the volume of the present epoch universe is dominated by voids (typically of diameter $\sim 30h^{-1}$ Mpc and smaller) which are separated and threaded by walls and filaments containing clusters of galaxies, the timescape model is based on two scales: the spatially flat wall regions which contain gravitationally bound structures, and the voids, which are negatively curved. Large gradients in Ricci scalar curvature are assumed to exist between the walls/filaments and the voids, consistent with observations that the latter have density contrasts close to $\delta\rho/\rho \sim -1$ (Hoyle & Vogeley 2002, 2004). At any location the local spatial curvature is in general different to any global average, and in order to make sense of average cosmological parameters this variance in local geometries must also be taken into account (Wiltshire 2007a). Observers in any region who try to fit a single FLRW geometry based on the mistaken assumption that the global spatial curvature is the same as the local value will determine different cosmological parameters.

As observers in galaxies, our local average geometry, up to a scale enclosing gravitationally bound galaxy clusters, is assumed to be spatially flat on average and marginally expanding at the boundary, with a FLRW–type geometry with scale factor a_{w},

$$\mathrm{d}s_{fi}^2 = -\mathrm{d}\tau^2 + a_{\mathrm{w}}^2(\tau)[\mathrm{d}\eta_{\mathrm{w}}^2 + \eta_{\mathrm{w}}^2\mathrm{d}\Omega^2]. \tag{1}$$

Finite infinity[3] (Ellis 1984), denoted *fi*, demarcates the

boundary between gravitationally bound and unbound systems (Wiltshire 2007a). The local geometry in the centre of voids is similarly assumed to be given by a negatively curved FLRW geometry with scale factor a_{v}, and a time parameter τ_{v} which does not in general coincide with τ.

The ensemble of void and wall regions is assumed to evolve by a Buchert average (Buchert 2000), with a volume–averaged scale factor

$$\bar{a}^3 = f_{\mathrm{vi}}a_{\mathrm{v}}^3 + f_{\mathrm{wi}}a_{\mathrm{w}}^3 \equiv \bar{a}^3(f_{\mathrm{v}} + f_{\mathrm{w}}), \tag{2}$$

where $f_{\mathrm{vi}} \ll 1$ is the initial void fraction, and $f_{\mathrm{wi}} = 1 - f_{\mathrm{vi}}$. The Buchert equations determine $\bar{a}^3$ in terms of an average volume expansion on spatial hypersurfaces comoving with the dust. Consequently the scale factor $\bar{a}$ is a statistical quantity which cannot be directly assigned any local geometrical meaning. It is therefore impossible to apply solutions of the Buchert equations to observed quantities to infer cosmological parameters until one provides: (i) an operational definition of what is to be understood by "dust"; and (ii) an operational means of relating a local average geometry such as (1) to the volume-average $\bar{a}$.

The operational interpretation of the Buchert formalism is not directly addressed in Buchert's original work (Buchert 2000), although the broad issues were discussed by Buchert & Carfora (2002, 2003). In the absence of a direct operational interpretation many authors have simply treated $\bar{a}$ as if it were the geometrical scale factor in an FLRW model, with corresponding cosmological parameters[4]. However, in the presence of strong inhomogeneities every observer cannot be the same average observer, and variance in local geometry can play an important role in parameter fitting. With this in mind, Wiltshire (2007a,b, 2008, 2009) adopts a fundamentally different approach to the operational interpretation of solutions to the Buchert equations.

Firstly, it is assumed that dust particles are coarse–grained on scales of order $100/h$ Mpc, on which there are no appreciable average mass flows. Although atomic sized dust is a perfectly valid description for cosmology at the epoch of last scattering, once stars and galaxies form the dust in cosmological models is typically coarse–grained on scales larger than that of galaxies, so that one need only deal with regions with the same sign of the expansion rate, neglecting the problems that arise when particle geodesics intersect and pressure becomes significant. By coarse–graining on scales on which average mass flows are not appreciable, we can consistently consider cosmic evolution from last scattering until the present epoch without having to consider energy fluxes which are not included in the energy–momentum tensor in Buchert's scheme.

Given the coarse scale on which dust "particles" are defined, we interpret Buchert's time parameter, t, as a collective degree of freedom of a dust particle, which does not necessarily coincide with the clock of an ideal isotropic observer, namely one who detects an isotropic cosmic microwave background (CMB). In particular, it is assumed that on account of quasilocal gravitational energy gradients isotropic observers in galaxies and voids have clock rates that develop a significant variance cumulatively over the lifetime of

---

[3] Ellis (1984) gave a qualitative definition of finite infinity. The definition adopted here (Wiltshire 2007a) is one possible realisation.

[4] See, e.g., Buchert et al. (2006); Räsänen (2006, 2008); Mattsson (2009); Larena et al. (2009); Wiegand & Buchert (2008); Mattsson & Mattsson (2010).

the universe. This means hypothetical observers in voids un-bound to any structures will ultimately measure a different mean CMB temperature from observers in galaxies. However, it does not affect cosmological observations directly, since on account of structure formation we and all the objects we observe are necessarily in regions of greater than critical density, which are contained within walls and keep a cosmic time in step with ours.

The Buchert time parameter, t, is then that carried by the clock of an isotropic observer in a region within a dust particle where the local spatial curvature happens to coincide with the volume–average spatial curvature. In a universe dominated in volume by voids, this will necessarily be in a void, though not at a void centre. The proper time of isotropic wall observers, τ, is related to t by the lapse parameter

$$\bar{\gamma} = \frac{\mathrm{d}t}{\mathrm{d}\tau}.$$

Although backreaction, arising from the variance of the relative expansion rates of the voids and walls with respect to any one set of clocks, is necessary to obtain apparent cosmic acceleration, for realistic cosmological parameters (Wiltshire 2007a; Leith et al. 2008; Wiltshire 2009) the backreaction is relatively small as a fraction of the total energy density ($< 5\%$). Thus in contrast to other approaches to Buchert averaging (Buchert 2008), apparent acceleration is not derived from backreaction alone. The crucial feature which leads to apparent acceleration for realistic cosmological parameters is the difference in clock rates between wall observers and the volume average, which can typically grow to the order of 38% by the present epoch (Leith et al. 2008).

To complete the operational interpretation of the solutions to the Buchert equation, the volume average scale factor $\bar{a}$ is adapted to a spherically symmetric average metric (Wiltshire 2007a)

$$\mathrm{d}s^2 = -\mathrm{d}t^2 + \bar{a}^2(t)\mathrm{d}\bar{\eta}^2 + A(\bar{\eta}, t)\mathrm{d}\Omega^2, \qquad (3)$$

in terms of the Buchert time parameter, where the area function A is defined by an average over the particle horizon volume (Wiltshire 2007a). An effective radial null cone average in terms of the parameters of the wall geometry is then obtained by conformally matching radial null geodesics of (1) and (3) adapted to a common centre, to relate the conformal time parameters η_{w} and $\bar{\eta}$ according to

$$\mathrm{d}\eta_{\mathrm{w}} = \frac{f_{\mathrm{wi}}^{1/3}\mathrm{d}\bar{\eta}}{\bar{\gamma}\left(1 - f_{\mathrm{v}}\right)^{1/3}} \qquad (4)$$

In place of (3), we then extend the metric (1) beyond finite infinity to obtain a spherically symmetric average cosmological metric adapted to wall clocks,

$$\mathrm{d}s^2 = -\mathrm{d}\tau^2 + a^2[\mathrm{d}\bar{\eta}^2 + r_{\mathrm{w}}^2(\bar{\eta}, \tau)\mathrm{d}\Omega^2] \qquad (5)$$

where $a \equiv \bar{a}/\bar{\gamma}$, and

$$r_{\mathrm{w}} \equiv \bar{\gamma}\left(1 - f_{\mathrm{v}}\right)^{1/3} f_{\mathrm{wi}}^{-1/3}\eta_{\mathrm{w}}(\bar{\eta}, \tau), \qquad (6)$$

with $f_{\mathrm{v}} \equiv f_{\mathrm{vi}}a_{\mathrm{v}}^3/\bar{a}^3$. It should be stressed that neither (3) nor (5) are exact solutions of the Einstein equations, but are effective average spherically symmetric geometries that represent a solution of the statistical Buchert average of the Einstein equations, when adapted to different clocks and rulers.

Given the two metrics (3) and (5), there are also different sets of cosmological parameters. The independent Buchert equations (Buchert 2000),

$$\bar{\Omega}_{\mathrm{m}} + \bar{\Omega}_{\mathrm{k}} + \bar{\Omega}_{\mathcal{Q}} = 1, \qquad (7)$$

$$\bar{a}^{-6}\partial_t\left(\bar{\Omega}_{\mathcal{Q}}\bar{H}^2\bar{a}^6\right) + \bar{a}^{-2}\partial_t\left(\bar{\Omega}_{\mathrm{k}}\bar{H}^2\bar{a}^2\right) = 0, \qquad (8)$$

deal with the volume–average or bare parameters, relative to the metric (3). Here $\bar{\Omega}_{\mathrm{m}} = 8\pi G\bar{\rho}_{M0}\bar{a}_0^3/[3\bar{H}^2\bar{a}^3]$, $\bar{\Omega}_{\mathrm{k}} = -k_{\mathrm{v}}f_{\mathrm{vi}}^{2/3}f_{\mathrm{v}}^{1/3}/[\bar{a}^2\bar{H}^2]$, and $\bar{\Omega}_{\mathcal{Q}} = -\dot{f}_{\mathrm{v}}^2/[9f_{\mathrm{v}}(1 - f_{\mathrm{v}})\bar{H}^2]$ are the bare matter, curvature and kinematic back-reaction parameters respectively, $\bar{H} \equiv \dot{\bar{a}}/\bar{a}$ is the volume–average or bare Hubble parameter, an overdot denotes a derivative w.r.t. volume–average time, t, and the average curvature is due to the voids only, which are assumed to have $k_{\mathrm{v}} < 0$. The bare Hubble parameter satisfies the relation

$$\bar{H} = f_{\mathrm{v}}H_{\mathrm{v}} + f_{\mathrm{w}}H_{\mathrm{w}}, \qquad (9)$$

where $H_{\mathrm{v}} \equiv \dot{a}_{\mathrm{v}}/a_{\mathrm{v}}$ and $H_{\mathrm{w}} \equiv \dot{a}_{\mathrm{w}}/a_{\mathrm{w}}$ are the regional average expansion rates of voids and walls, with respect to volume–average time. It is convenient to define $h_r(t) \equiv H_{\mathrm{w}}/H_{\mathrm{v}} < 1$.

Relative to the metric (5), one can also define dressed parameters, which will take numerical values similar to those of cosmological parameters in the FLRW models. Such parameters do not satisfy a relation such as (7), however. The most relevant are the dressed matter density parameter

$$\Omega_{\mathrm{m}} = \bar{\gamma}^3\bar{\Omega}_{\mathrm{m}}, \qquad (10)$$

and the dressed Hubble parameter

$$H \equiv \frac{1}{a}\frac{\mathrm{d}a}{\mathrm{d}\tau} = \bar{\gamma}\bar{H} - \frac{\mathrm{d}}{\mathrm{d}t}\bar{\gamma} = \bar{\gamma}\bar{H} - \bar{\gamma}^{-1}\frac{\mathrm{d}}{\mathrm{d}\tau}\bar{\gamma}. \qquad (11)$$

The present epoch value of the dressed Hubble parameter will coincide with the standard Hubble constant, H_0, that we infer observationally from measurements averaged over both voids and walls on scales larger than the scale of statistical homogeneity.

One feature of the TS model that is particularly relevant for the analysis of luminosity distance data is that below the scale of statistical homogeneity we will expect to see significant variance in the Hubble flow. With respect to any one set of clocks the underdense voids expand faster than the more dense walls. Since voids dominate the volume of the universe, if we average only on nearby scales we will typically measure a higher value of the Hubble constant than the global average, H_0. A measurement confined to our own local wall, e.g., towards the Virgo cluster, would produce a lower value[5]. As we look out to greater and greater distances, a typical line of sight will eventually intersect as many walls and voids as the global average. Suppose that we perform a spherically symmetric average over the sky to try to determine the Hubble constant using only nearby measurements within some given finite maximum radius, which

---

[5] While this agrees with observation, astronomers typically talk about "Virgo–centric infall" rather than the expansion rate being less in regions of greater density. It is our view that such language, which derives from a conceptual framework of Newtonian gravitational forces in a static space, is inappropriate on scales over which the volume of space is expanding and therefore not well described by a static Euclidean geometry. One should not talk about "infall" unless the distance between two objects is actually decreasing.

is then varied. The Hubble "constant" inferred in this manner should peak at the dominant void scale $30/h$ Mpc, i.e. at $z \sim 0.01$, with a maximum value up to 17% greater than the global average and then steadily decrease to near the global average value when the scale of statistical homogeneity is reached. The latter scale, which coincides with our scale for the coarse–graining of dust, is about $100/h$ Mpc. These expectations are consistent with the recent data analysis of Li & Schwarz (2008), and future observations would have the potential to either rule out or strongly constrain the TS scenario.

Since the scale of statistical homogeneity represents a redshift of order $z \sim 0.033$, and since many supernovae datasets contain a large number of supernovae below this scale, there are many potential systematic issues to consider. Such issues were not considered by Kwan et al. (2009), and will represent an important ingredient in our reanalysis.

Provided we are sampling distance scales *beyond* the scale of statistical homogeneity, then the luminosity distance for wall observers is given by (Wiltshire 2007a)

$$d_L = a_0(1+z)r_{\rm w}, \qquad (12)$$

where $r_{\rm w}$ may be determined from (4) and (6).

The general solution for the two–scale average of the Buchert equations was given by Wiltshire (2007b), and is expressed in terms of transcendental equations. It has four free parameters, two of which may be expressed as the initial void fraction, $f_{\rm vi}$, and the initial velocity dispersion $h_r(t_{\rm i})$. For initial conditions at last scattering consistent with the CMB we take initial values $10^{-5} < f_{\rm vi} < 10^{-2}$, $1 - h_r(t_{\rm i}) = 10^{-5}$. However, it turns out that the general solution is relatively insensitive to these values, as there is an attractor solution with $h_r(t) = \frac{2}{3}$ exactly, which the general solutions approach to within 1% by redshifts $z \sim 37$ (Wiltshire 2007b). The solutions then depend effectively on two free parameters, which can be taken to be the dressed Hubble constant and dressed matter density parameter at the present epoch.

For the tracker solution the dressed matter density parameter and void fraction at the present epoch are related by

$$\Omega_{\rm m0} = \frac{1}{2}(1 - f_{\rm v0})(2 + f_{\rm v0}). \qquad (13)$$

Furthermore, for the tracker solution, (4), (6) and (12) simplify to give (Wiltshire 2009)

$$\begin{aligned} d_L &= (1+z)^2 t^{2/3} \int_t^{t_0} \frac{2\,{\rm d}t'}{(2 + f_{\rm v}(t'))(t')^{2/3}} \\ &= (1+z)^2 t^{2/3} (\mathcal{F}(t_0) - \mathcal{F}(t)) \end{aligned} \qquad (14)$$

where

$$\begin{aligned} \mathcal{F}(t) &\equiv 2t^{1/3} + \frac{b^{1/3}}{6} \ln \left(\frac{(t^{1/3} + b^{1/3})^2}{t^{2/3} - b^{1/3}t^{1/3} + b^{2/3}} \right) \\ &\quad + \frac{b^{1/3}}{\sqrt{3}} \tan^{-1} \left(\frac{2t^{1/3} - b^{1/3}}{\sqrt{3}\,b^{1/3}} \right), \end{aligned} \qquad (15)$$

and $b \equiv 2(1 - f_{\rm v0})(2 + f_{\rm v0})/(9 f_{\rm v0} \bar{H}_0)$. For the tracker solution wall time is related to volume–average time by

$$\tau = \frac{2}{3}t + \frac{4\Omega_{\rm m0}}{27 f_{\rm v0} \bar{H}_0} \ln \left(1 + \frac{9 f_{\rm v0} \bar{H}_0 t}{4\Omega_{\rm m0}} \right), \qquad (16)$$

and the bare Hubble constant to the dressed Hubble constant by

$$\bar{H}_0 = \frac{2(2 + f_{\rm v0})H_0}{4f_{\rm v0}^2 + f_{\rm v0} + 4}. \qquad (17)$$

In the data analysis that follows, we used both the exact solution with $f_{\rm vi} = 10^{-4}$ and $h_r(t_{\rm i}) = 0.99999$ at $z = 1100$, and the tracker solution, and found that they gave essentially identical results to the accuracy quoted.

3 SUPERNOVA IA DATA REDUCTION METHODS

In this paper we consider two SN Ia light curve fitters. Current fitting methods descend from those used in the original discoveries of cosmic acceleration in 1998/1999: The Multicolor Light Curve Shape fitter MLCS2k2 (Jha, Riess & Kirshner 2007) is the most recent incarnation of the LCS fitter used by the High-Z Supernova Team (Riess et al. 1998), and the SALT/SALT II (Spectral Adaptive Light curve Template) fitters (Guy et al. 2005, 2007) improve the magnitude calibration based on the width-luminosity relation used by the Supernova Cosmology Project (Perlmutter et al. 1998).

Each method results in a distance modulus for each supernova. However, distance moduli computed for the same objects by the two fitting methods are not necessarily equal, due in large part to the different treatment of systematic uncertainties – in particular, colour variation due to dust extinction. It is very important when estimating cosmological parameters from the data from various SN Ia observation programmes that the data reduction process is consistent across the whole dataset.

When one is investigating an alternative cosmological model with SNe Ia, it is also vital to recognise that model dependence is introduced into the cosmological parameter estimation at different points in the data reduction process. We now compare the MLCS2k2 and SALT/SALT II algorithms in preparation for using their output distance moduli to test the timescape model. More thorough comparisons of these methods can be found in Hicken et al. (2009) and in Kessler et al. (2009).

3.1 MLCS2k2

For each supernova, MLCS2k2 returns a distance modulus $\mu = 5\log_{10}(d_L/10 \text{ pc})$ and its uncertainty via the MLCS2k2 model magnitude (Jha et al. 2007)

$$\begin{aligned} m_{\rm model}^{e,f} &= M^{e,f'} + \mu + p^{e,f'}\Delta + q^{e,f'}\Delta^2 \\ &\quad + X_{\rm host}^{e,f'} + X_{\rm MW}^{e,f} + K_{f,f'}^e. \end{aligned} \qquad (18)$$

A model magnitude is fitted at each time point (indexed by e, and defined relative to the time of maximum brightness), and for each observer-frame filter index f. The model is defined in *UBVRI* rest frame filters f', with the light curve shape parameter Δ representing the relation between luminosity and duration. Extinction due to dust is divided into host galaxy $X_{\rm host}$ and Milky Way $X_{\rm MW}$ components, and $K_{f,f'}$ is the K-correction between rest-frame and observer-frame filters. Obtaining a set of distance moduli takes two steps. One first computes the model vectors $M^{e,f'}$, $p^{e,f'}$, and $q^{e,f'}$ by minimising the distance modulus residuals of

a training set of nearby SN Ia, which lie within the range in which the Hubble line is linear, yet are sufficiently distant for their peculiar velocities to be negligible compared with their Hubble-flow velocity. Secondly, one fits for the distance moduli along with the remaining parameters, on the assumption that SNe Ia at higher redshifts are identical to those nearby.

The extinction terms are set up independently of these fits. There is some colour dependence on the brightness incorporated in Δ, but there is also a significant colour dependence on extinction by dust in the host galaxy and in the Milky Way. Following Cardelli, Clayton & Mathis (1989), MLCS2k2 characterizes the extinction by first defining $\zeta^{e,f'} \equiv X^{e,f'}/A_0^{e,f'}$, where $A_0^{e,f'}$ is the extinction in passband f' at maximum light in B. Hence, $\zeta^{e,f'}(t=0)$ is defined to be 1, and $\zeta^{e,f'}$ encapsulates the time dependence of the exinction. Then one fits for the coefficients $\alpha^{f'}$ and $\beta^{f'}$, defined by

$$X^{e,f'} = \zeta^{e,f'}\left(\alpha^{f'} + \frac{\beta^{f'}}{R_V}\right)A_V^0, \qquad (19)$$

at maximum light, where R_V is the ratio of the extinction in the V-band to the colour excess $E(B-V)$. A "Milky Way-like" reddening law, based on an average over a number of lines of sight, has $R_V = 3.1$. This has conventionally been assumed to apply also in SN Ia host galaxies. However, Hicken et al. (2009) and Kessler et al. (2009) find that this value for R_V *overestimates* host galaxy extinction. The question of how to parameterise the extinction is complicated by a degeneracy with Hubble bubble assumptions (Conley et al. 2007). Different groups use different values.

There are four model parameters for each SN Ia: the distance modulus μ; the time of peak luminosity in the rest-frame B-band; the shape-luminosity parameter Δ; and host galaxy extinction A_V. The estimates and uncertainties of each parameter value are determined by marginalizing over the three other parameter probability distribution functions and taking the mean and rms of the resulting probability distribution for the parameter of interest.

With a distance modulus and its uncertainty for each supernova, cosmological parameter estimates are obtained by minimizing the χ^2 statistic:

$$\chi^2 = \sum_i \frac{[\mu_i - \mu(z_i, H_0, \Omega_{m0})]^2}{\sigma_{\mu_i}^2} \qquad (20)$$

where $\mu(z_i, H_0, \Omega_{m0})$ is the theoretical distance modulus calculated for the redshift of the i-th SN Ia, based on a set of cosmological parameters H_0 and Ω_{m0} for a spatially flat universe.

3.2   SALT/SALT II

Whereas the MLCS calibration uses a nearby training set of SNe assuming a close to linear Hubble law, SALT (Guy et al. 2005) uses the whole dataset to calibrate empirical light curve parameters. SNe Ia from beyond the range in which the Hubble law is linear are used, so a cosmological model must be assumed in this method. Typically the ΛCDM model is assumed. To deal with a determination of empirical parameters for objects at unknown distances, the absolute magnitude M and H_0 are combined as

$$\mathcal{M} = M - 5\log_{10} h + 5\log_{10} c + 10. \qquad (21)$$

The distance modulus is then modeled as

$$\mu_i = m_{B_i}^{\max} - \mathcal{M} + \alpha(s_i - 1) - \beta c_i. \qquad (22)$$

The initial light curve standardization results in best fit values for the time of maximum B-band light, t_0, the rest-frame peak magnitude in the B-band, $m_B^{\max}$, a stretch factor s, and a colour parameter c, in which are combined the intrinsic supernova colour and reddening due to dust in its host galaxy.

SALT II (Guy et al. 2007) builds on SALT by including spectroscopic information to improve the wavelength resolution of the spectral templates. We use the relationship between the SALT stretch parameter s and the SALT II parameter x_1 given in Guy et al. (2007) in order to compute cosmological parameters for SALT II SNe Ia with the same program as we use for the SALT SNe Ia.

In MLCS2k2, the cosmological parameter estimation step is "decoupled" from the distance modulus determination. In SALT, after obtaining the parameters s and c for each SN Ia from the light curve fits, a *magnitude* for each supernova is fitted via the equivalent expression to eq. (20), and the cosmological parameters are obtained as part of the same minimization, viz.

$$\chi^2 = \sum_i \frac{[m_{Bi} - m(z_i; \alpha, \beta, \mathcal{M}, \Omega_{m0})]^2}{\sigma_{m_i}^2}. \qquad (23)$$

This process results in global estimates of α, β, and $\mathcal{M}$, and a corresponding Ω_{m0}. An additional "intrinsic" dispersion is introduced to the SN Ia absolute magnitudes such that one obtains a reduced χ^2 of 1 for the best fit set of parameters (Guy et al. 2007). Consequently the published tables of SN Ia distance moduli obtained with the SALT/SALT II fitters retain a degree of model dependence. In the case of the Union and Constitution datasets, the quoted distance moduli were computed for a spatially flat (FLRW) universe with a constant w.

There are many subtleties in the individual implementations of the SNe Ia reduction. The cosmological parameters computed for the Union dataset of Kowalski et al. (2008) are obtained from the χ^2 equation (23) above, but with additional nuisance parameters encoding the propagating systematic uncertainties (see their equation (5)).

3.2.1   Combining datasets

Since SALT uses the whole dataset, the global parameter minimization needs to be rerun when new data is added. When they augment the Union set with the nearby CfA3 SNe Ia to produce the Constitution dataset, Hicken et al. (2009) first take the SALT parameters of the Union dataset, $m_B^{\max}$, s, and c, "out of the box" and calculate a best-fit cosmology incorporating a BAO prior in the cosmological fit: $\chi^2 = \chi_\mu^2 + \chi_{BAO}^2$. The reason for this was presumably that the BAO prior constrains the range of Ω_{m0} better than the SNe Ia alone, and thus provided a more stringent assurance that the new cosmological parameter estimation was in line with the old one. Once the Union results were reproduced with sufficient accuracy, the light curves of nearby Union SNe Ia were run once again through SALT to ensure that

the new m_B^{max}, s, and c values agreed with the Union ones, and then the whole CfA3 sample was run through SALT, so that it could be combined with the Union set without introducing any significant offset. The uncertainty in the distance modulus σ_μ was calculated by Hicken et al. (2009) in a way that differs from Kowalski et al. (2008). Essentially, the σ_μ calculated by Hicken et al. (2009) contains adjustments that ensure reproduction of the same uncertainty in w as in Kowalski et al. (2008).

If one wishes to test a non-standard cosmological model using SALT SNe Ia, as in the present study, the minimization process in eq. (20) should at the very least be recalculated with the appropriate luminosity distance formula to determine the empirical light curve parameters. However, for consistency, the assumptions underlying the determination of the uncertainties in the χ^2 minimization procedure should ideally also be carefully rethought. The analysis must be consistent across both standard and non-standard cosmological models in order to produce a meaningful Bayes factor. From the standpoint of the non-standard model, when combining datasets as above one can no longer simply manipulate the uncertainties in such a way that published constraints for the parameter w of the standard cosmology are more or less reproduced.

3.3   Systematic uncertainties

It has been noted in several studies, (e.g., Hicken et al. (2009); Kessler et al. (2009); Komatsu et al. (2010)), that there are possible discrepancies between SALT- and MLCS-reduced datasets, and also between different implementations of the same fitters. This is a significant issue for our investigation.

One direct way of quantifying the differences is to compare the published distance moduli for the 140 SNe Ia common to the Riess07, Union and Constitution datasets. In Fig. 1 we plot the differences between the published Riess07 and Constitution distance moduli for the 140 data points they have in common. This shows that $|\mu_{Gold} - \mu_{Const}| \lesssim$ 1 mag. Individually these differences are quite significant in some cases. However, the differences show no obvious redshift-dependent trend so they should not bias the relative estimates of cosmological parameters.

One should be careful not to draw the conclusion that the differences seen in Fig. 1 are only to be found in comparing MLCS (used in the Riess07 gold sample) with SALT (used in the Constitution sample). As discussed above, when using the SALT fitter a global refit of all the empirical light curve and cosmological parameters is required when extra data is included in a sample. To illustrate the effect of this, we have taken the same 140 SNe Ia common to the Riess07, Union and Constitution datasets and have computed a SALT fit to this subsample directly, assuming a spatially flat ΛCDM model, using Conley's publicly available `simple_cosfitter` code[6]. In Fig. 2 we display the differences between these distance moduli and the corresponding distance moduli of the same SNe Ia events as published in the Constitution compilation. We see that the resulting scatter is half of that in Fig. 1, even though the SALT method

---

Figure 1. Differences in published distance moduli between the 140 SNe Ia common to the Riess07 gold sample and the Constitution sample, as a function of redshift.
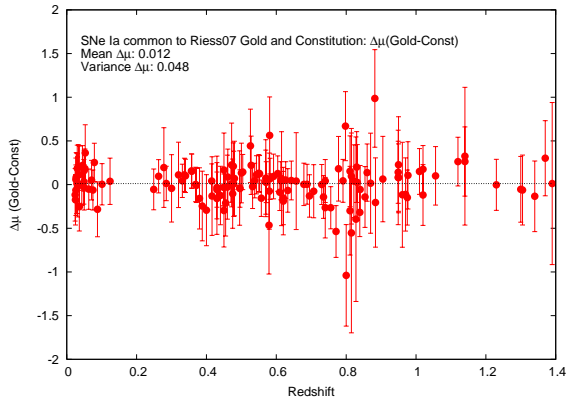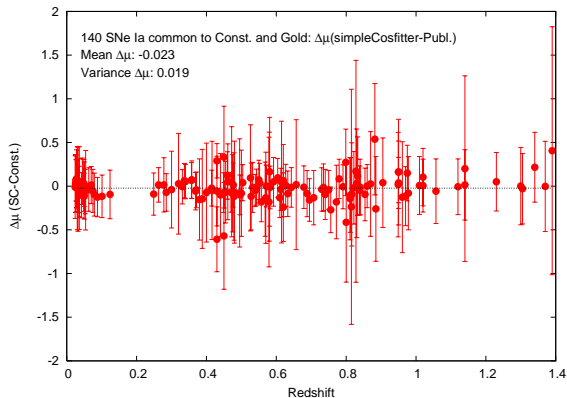

Figure 2. Differences in distance moduli between values published in the Constitution sample, and the corresponding values determined with `simple_cosfitter` (ΛCDM) using only the subsample of 140 SNe Ia plotted in Fig. 1, as a function of redshift. $H_0 = 65$ km s^{-1} Mpc^{-1} .

has been applied in each case. This is due to the variation in the values of the parameters α, β and M_B determined from only 140 SNe Ia in the subsample, as compare to those determined from all 397 SNe Ia in the full sample.[7]

Much more detailed studies of these sorts of issues have already been conducted by various researchers, revealing a complex picture.

In their comparison of the different fitters, Hicken et al. (2009) found that SALT, SALT II, and MLCS2k2 produce light curve shape and color/reddening parameters that agree well with each other and that it is in determining the distance modulus that systematic offsets are introduced. For example, SALT produces more scatter at high redshifts than MLCS2k2, and the nearby MLCS17 distances are larger

---

[6] `http://qold.astro.utoronto.ca/conley/simple_cosfitter/`

[7] Since the `simple_cosfitter` implementation of SALT is not perfectly identical to that used by Hicken et al. (2009), as a check we reran `simple_cosfitter` on the full Constitution sample. The difference between the published fits and those computed with `simple_cosfitter` are indeed insignificant, as is shown in Fig. 3.

Figure 3. Differences in distance moduli between published values in the Constitution sample, and values determined with `simple_cosfitter` (ΛCDM) using the full Constitution sample, as a function of redshift. $H_0 = 65$ km s^{-1} Mpc^{-1} .
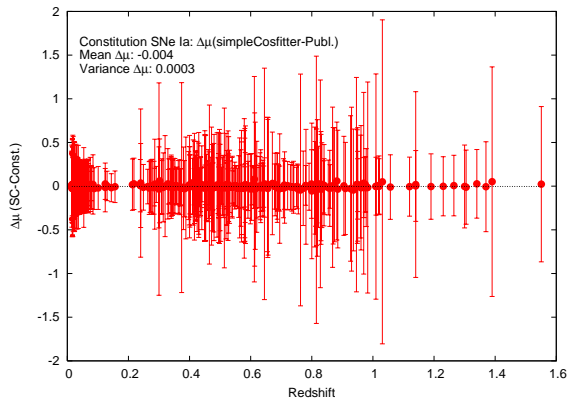
than in SALT. Such discrepancies will clearly affect the cosmological parameter fits. Hicken et al. (2009) note that although there exist some trends in the $\mu(\text{MLCS17}) - \mu(\text{SALT})$ differences versus shape parameter Δ and color parameter β, there are no trends versus redshift, which would indicate the influence of hidden systematics and affect the cosmological parameter fits (Wood-Vasey et al. 2007). These are grounds for hope that retraining with larger datasets, combined with a better treatment of systematic uncertainties, will reconcile the differences. In the meantime, however, they found that for the best cut samples, SALT and SALT II estimates of w differ by 0.05–0.09 from the MLCS estimates.

After accounting for an anomaly in the rest-frame U-band that affects the nearby SNe Ia with the SALT II fitter and all except the nearby sample with the MLCS2k2 fitter, Kessler et al. (2009) found a discrepancy of 0.31 in the value of w estimated from one of their MLCS2k2 sample combinations as compared to that of the corresponding sample from the MLCS2k2 ESSENCE collaboration(Wood-Vasey et al. 2007). They show that this is due to different parameterisations of the dust extinction term in different implementations of MLCS2k2.

When constraining dark energy parameters derived from WMAP7+BAO+SN, Komatsu et al. (2010) found that the parameters of the minimal 6-parameter ΛCDM model changed depending on whether the SN Ia compilation used SALT II or MLCS2k2 based on the SN sample of Kessler et al. (2009). They noted that it is not presently obvious how to properly incorporate systematic uncertainties into the likelihood analysis and thereby reconcile different methods and datasets. Komatsu et al. (2010) use the Constitution sample when quoting canonical cosmological parameter values, because it is an extension of the Union sample which they used for the 5-year WMAP analysis.

3.3.1 *The Hubble bubble*

In addition to the general question of the effect of unknown systematics on cosmological parameters, there is one particular systematic which is of interest for the TS model, namely the possible existence of a Hubble bubble. As discussed in

Sec. 2 it is a feature of the TS model that we will observe an apparent increase in the value of the Hubble constant on scales less than the scale of statistical homogeneity at $z \sim 0.033$. A spherically symmetric average of the Hubble rate over increasing local volumes will give a peak variance of order 17% above the mean on scales $z \sim 0.01$, which then steadily decreases until the scale of statistical homogeneity is reached.

Usually, very low redshift objects are left out of SNe Ia samples because their peculiar velocities are a considerable fraction of their Hubble flow velocities, but depending on the sample events with redshifts $z \gtrsim 0.01$ have been included. Evidence of a Hubble bubble was found by Zehavi et al. (1998), and confirmed by Jha et al. (2007), using a MLCS2k2 sample with $R_V = 3.1$. Modeling the expansion law in terms of a single inner region void expanding faster than the outer FLRW region, they found a drop in the Hubble constant of $\delta_H = (H_{\text{inner}} - H_{\text{outer}})/H_{\text{outer}} = 0.065$ at a redshift $z = 0.024$. However, there exists a degeneracy between the existence of such a small scale Hubble bubble and the treatment of reddening/extinction (Conley et al. 2007).

In the SALT-reduced samples, a Hubble bubble is found if $\beta = 4.1$ is assumed – which is believed to roughly correspond to the CCM89 value for reddening in the Milky Way – but disappears if $\beta < 4.1$ (Conley et al. 2007). With their MLCS31 sample (366 SNe Ia) Hicken et al. (2009) find 5.56σ evidence for a void at $z = 0.028$ with reduced amplitude $\delta_H = 0.029$. In their MLCS17 sample (372 SNe Ia) by contrast, with $R_V = 1.7$, they find 2.75σ evidence for a negative void at $z = 0.034$ with $\delta_H = -0.020$.

It is clear that unknown systematic uncertainties in reddening and extinction of supernovae in their host galaxies will lead to different results regarding local inhomogeneities. Different groups have made different choices about the minimum cutoff in light of these uncertainties. Riess et al. (2007) took a minimum redshift $z = 0.024$, whereas Hicken et al. (2009) included data down to $z = 0.01$. By contrast, Kessler et al. (2009), for their full MLCS2k2 Nearby+SDSS+SNLS+ESSENCE+HST sample, took a minimum redshift of $z = 0.0218$, based on the midpoint of a ± 0.06 variation in w with minimum redshift cuts between 0.01 and 0.03.

The statistical nature of the apparent Hubble expansion law expected in the TS model will differ from the empirical models used in the above analyses of the Hubble bubble, as we are not dealing with a uniformly expanding void inside a background region. However, in general an increased minimum redshift cut[8] should be made in the TS model, a point to which we will return in Sec. 4.3.

3.4 The value of H_0 and cosmological fits

The overall normalisation of the luminosity distance depends on the value of the Hubble constant, H_0. However, one cannot extract information about the value of the Hubble con-

---

[8] The effects of minimum redshift cuts have also recently been discussed for the Hubble bubble generated by single–void Lemaître–Tolman–Bondi models (Sinclair, Davis & Haugbølle 2010). This will also have different characteristics to the apparent Hubble bubble in the TS model.

stant independently of a knowledge of the intrinsic luminosity of standard candles, since uncertainties in the parameters M and H_0 are degenerate with one another in the distance modulus. The SALT fitter provides a global estimate of $\mathcal{M}$ in which any uncertainties are combined according to (21), and so say nothing about the value of H_0 directly. The value of H_0 must be determined by an independent calibration.

In the MLCS method, the overall distance scale similarly relies on the calibration of the magnitudes of nearby SNe Ia, usually to the Cepheid distance scale (Freedman et al. 2001; Sandage et al. 2006; Riess et al. 2009).

It is impossible therefore to infer the value of the Hubble constant by a fit to SNe Ia data alone. However, for the MLCS method, in which the uncertainties in the intrinsic magnitudes have hopefully already been accounted for, the fit of luminosity distances to a particular cosmological model can nonetheless provide an estimate of the variance in H_0 values that are admissible for that model, given a particular SNe Ia dataset. Since independent cosmological tests, such as the determination of the angular diameter distance of the sound horizon, or of the comoving baryon acoustic oscillation scale, lead to different constraints on H_0, in order to compare the potential agreement of different tests Leith et al. (2008) plotted confidence levels for the fit to the Riess07 gold data in their Fig. 2, using the normalization assumed in the data[9]. One should bear in mind that these confidence limits can be translated up or down the H_0-axis, depending upon what overall normalization is assumed for the Hubble constant.

Constraints on the Hubble constant from WMAP and baryon acoustic oscillations in the TS model were given in Fig. 2 of Leith et al. (2008) and are reproduced in Fig. 4. The constraints from WMAP are estimated by fitting the angular scale of the sound horizon to within 2, 4 or 6%. The BAO constraints are similarly estimated by assuming that the dressed comoving scale of the sound horizon matches the corresponding scale of $104\,h^{-1}$ Mpc for the ΛCDM model to within 2, 4 or 6%. Assuming that these estimates roughly correct[10] then Fig. 4 shows that values of $57 \lesssim H_0 \lesssim 68\,\mathrm{km\ sec^{-1}\,Mpc^{-1}}$ would be admissible in the TS scenario, but values as large as the recent $H_0 = 74.2 \pm 3.6\,\mathrm{km\ sec^{-1}\,Mpc^{-1}}$ determined by the SH0ES survey (Riess et al. 2009) would represent a severe challenge to the model.

The determination of the value of the Hubble constant is a complex problem from the viewpoint of the TS model,

---

[9] Riess et al. (2007) did not state what value of H_0 was assumed in their dataset, but stated that a systematic subtraction of 0.32 mag from their distance moduli would match the Cepheid calibration of Riess et al. (2005). The question of the Cepheid calibration is a matter of debate (Sandage et al. 2006; Riess et al. 2009). Since a fit of the spatially flat ΛCDM model to the unmodified Riess07 SNe Ia distance moduli gives a value $H_0 = 62.6 \pm 1.4\,\mathrm{km\ sec^{-1}\,Mpc^{-1}}$ consistent with the value determined by Sandage et al. (2006), Leith et al. (2008) chose to use the unmodified distance moduli of Riess et al. (2007). The recent Cepheid calibration of Riess et al. (2009) is in disagreement with the Sandage et al. (2006) calibration.

[10] A direct comparison with the data requires that we compute the expected angular anisotropy power spectrum for the TS model in the case of the CMB, and also that all model dependent assumptions in the data reduction of galaxy clustering data are carefully re-examined in the case of the BAO analysis.

Figure 4. Parameter values in the $(\Omega_{\mathrm{m0}}, H_0)$ plane which fit the angular scale of the sound horizon $\delta = 0.01$ rad deduced for WMAP (Bennett et al. 2003; Spergel et al. 2007), to within 2%, 4% and 6% (contours running top–left to bottom–right); as compared to parameters which fit the effective comoving scale of $104h^{-1}$Mpc for the baryon acoustic oscillation (BAO) observed in galaxy clustering statistics (Cole et al. 2005; Eisenstein et al. 2005), to within 2%, 4% and 6% (contours running bottom–left to middle–right) which fit the angular diameter dis of Gold07 (Table 8), SDSS-II (Table 6), MLCS17 and MLCS31 (Table 9). In each case an overall normalization of the Hubble constant from the published dataset is assumed.
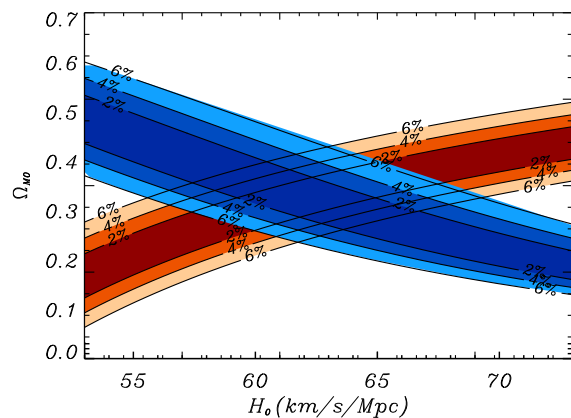
given that many of the crucial measurements are made below the scale of statistical homogeneity, over scales on which the local Hubble flow should exhibit quite large variability. Indeed, the statistical properties of the observed fractional variability of the Hubble flow (Li & Schwarz 2008) do seem broadly consistent with the expectations of the TS scenario. For concordance of the geometrical tests of average cosmological parameters, the real challenge is the baseline value of H_0, however.

Ideally the global average Hubble constant should be determined only on scales significantly larger than the scale of statistical homogeneity, $z > 0.033$, by methods which do not depend on calibrations below that scale. The method of determining H_0 via the time delays of multiply-imaged quasars in strongly gravitationally-lensed systems fulfils this criteria. This method has given a large variety of estimates for H_0 (Oguri 2007). A recent new estimate of H_0 from accurate time delay measurements with six years of data from the quadruply imaged quasar HE 0435-1223 gives $H_0 = 62^{+6}_{-4}\,\mathrm{km\ sec^{-1}\,Mpc^{-1}}$ (Courbin et al. 2010). In considering such estimates from the perspective of the TS model, one must be careful to examine any assumptions which might assume the standard cosmology.

The analysis of the Sunyaev–Zel'dovich effect and X–ray data of galaxy clusters provides another method of constraining H_0 independently of calibration to standard candles in the extragalactic distance ladder Reese et al. (2010). If the standard ΛCDM angular diameter distance is replaced by that of the TS model then this method could be easily adapted to give further constraints in the $(H_0, \Omega_{\mathrm{m0}})$ parameter space. This is beyond the scope of the present paper, and will be left to future work.

Since we are not interested in the comparing other cosmological tests in this paper, we will not consider the question of the value of H_0 further. Rather we will concentrate on the comparison of the expansion history for the TS and spatially flat ΛCDM models as determined by the luminosity distances of various SNe Ia datasets.

4   SUPERNOVA ANALYSIS OF THE TIMESCAPE MODEL

In this section we will test the TS model against all available datasets. In view of the systematic uncertainties it is important that we consider the effects of using the different fitters, as well as additional possible systematic effects specific to the TS model. In § 4.1, we discuss TS fits to the published datasets "out of the box". In § 4.2, we determine the extent to which substitution of the TS luminosity distance calculation for the ΛCDM one in the simple_cosfitter code affects parameter estimation. We then investigate the effects of making sample cuts according to the redshift corresponding to the scale of statistical homogeneity in § 4.3. Finally, in § 4.4 we discuss some systematic issues relevant to MLCS2k2.

4.1   "Out of the box" data

Kwan et al. (2009) simply took the published values of the Union and Constitution datasets, produced data fits and concluded that the TS model was a relatively poor fit, with the implication that the TS failed when presented with the newer larger datasets. However, as we discussed above, given that the Union and Constitution datasets are fit by SALT, which implicitly assumes a homogeneous isotropic cosmology to all distances in its data reduction, serious concerns arise in using the SALT method. In fact, it was for this reason that the MLCS–reduced data of Riess07 was used by Leith et al. (2008) in preference to SALT–reduced SNLS data.

For the purpose of subsequent comparison, we will first collate TS cosmological parameter fits for all available datasets in Table 1 using the data "out of the box". The three datasets investigated in this manner by Kwan et al. (2009) were the Riess07 gold data (Riess et al. 2007), and the SALT-fitted Union (Kowalski et al. 2008) and Constitution (Hicken et al. 2009) datasets. To these we add the equivalent parameter fits for the SALT2, MLCS17 and MLCS31 datasets of Hicken et al. (2009), the 288-SN Ia Nearby+SDSS+ESSENCE+SNLS+HST sample of Kessler et al. (2009), and the 557-SN Ia Union2 sample of Amanullah et al. (2010). The MLCS17 and MLCS31 datasets share many SNe Ia in common with the Constitution set, but were fitted by MLCS2k2 with values for the extinction parameter R_V of 1.7 and 3.1 respectively. The value $R_V = 1.7$ was found by Hicken et al. (2009) to give less scatter in the Hubble residuals for a sample of nearby SNe Ia, in keeping with previous studies which found the colour parameter β in eq. (22) to be significantly lower than would be expected if the host galaxy reddening law conforms to a Milky Way reddening law ($R_V = 3.1$). The SDSS-II data (Kessler et al. 2009) was fitted by MLCS2k2 with $R_V = 2.18$. The Union2 dataset is fit with SALT II.

Table 1. Expectation values for the parameters for the timescape model from SNe Ia data, using published SNe Ia data as selected and reduced by the respective SNe Ia collaborations. The bestfit value of Ω_{m0} is quoted in brackets in addition to the expectation value. The MLCS17, MLCS31, and SALT2 datasets were published along with the Constitution dataset in Hicken et al. (2009). The SDSS-II dataset is the full 288-object dataset described in Kessler et al. (2009) and available from http://das.sdss.org/va/SNcosmology/sncosm09_fits.tar.gz. The sample size, N, and minimum χ^2 are also tabulated. S=SALT; S2=SALT2; M=MLCS2k2.

Dataset	N	χ^2	Ω_{m0}	f_{v0}
Riess07 (M)	182	162.7	$0.29^{+0.14}_{-0.13}(0.33)$	$0.79^{+0.11}_{-0.12}$
Union (S)	307	319.6	$0.12^{+0.14}_{-0.12}(0.09)$	$0.91^{+0.09}_{-0.08}$
Const. (S)	397	470.8	$0.10^{+0.08}_{-0.09}(0.01)$	$0.93^{+0.06}_{-0.06}$
MLCS17 (M)[1]	372	403.1	$0.18^{+0.12}_{-0.15}(0.20)$	$0.87^{+0.09}_{-0.10}$
MLCS31 (M)[1]	366	432.8	$0.07^{+0.04}_{-0.06}(0.01)$	$0.95^{+0.02}_{-0.04}$
SALT2 (S2)[1]	352	346.8	$0.11^{+0.11}_{-0.10}(0.04)$	$0.92^{+0.08}_{-0.07}$
SDSS-II (M)[2]	288	240.8	$0.38^{+0.11}_{-0.09}(0.40)$	$0.72^{+0.05}_{-0.05}$
Union2 (S2)[3]	557	550.9	$0.08^{+0.05}_{-0.07}(0.01)$	$0.95^{+0.03}_{-0.04}$

[1]Hicken et al. (2009) [2]Kessler et al. (2009) [3]Amanullah et al. (2010)

Table 2. Published values for Ω_{m0} for the ΛCDM model from SNe Ia data, for comparison with Table 1. The Constitution value of Ω_{m0} includes a BAO prior. The SDSS-II value includes BAO and WMAP5 priors. Distance normalisation is arbitrary.

Dataset	N	χ^2	Ω_{m0}
Union	307	310.8	$0.29^{+0.05}_{-0.04}$
Constitution	397	—	$0.28^{+0.04}_{-0.02}$
SDSS-II[1]	288	237.9	$0.31^{+0.02}_{-0.02}$
Union2[2]	557	—	$0.274^{+0.040}_{-0.037}$

[1]These values come from table 13 in Kessler et al. (2009). [2]Statistical and systematic uncertainties combined.

We have compiled Table 1 by our own analysis of the data, with the prior[11] $0.01 \leqslant \Omega_{m0} < 0.95$ used by Kwan et al. (2009). For comparison, Table 2 shows ΛCDM parameter values that were published with the respective datasets.

The parameter values quoted by Leith et al. (2008) and Kwan et al. (2009) were those corresponding to the peak in the probability distribution, at which the χ^2 statistic is minimised. However, as Fig. 1 of Kwan et al. (2009) illustrates, for the published Union and Constitution datasets the best-fit value is driven to the edge of the parameter space at

---

[11] Kwan et al. (2009) state that this prior corresponds to taking a prior $10^{-5} < f_{vi} < 10^{-2}$ on the void fraction at last scattering. However, while the value of Ω_{m0} is closely related to f_{v0}, it is essentially independent of f_{vi} on account of the existence of the tracker solution. Leith et al. (2008) used the value $f_{vi} = 10^{-4}$ with the exact solution for *all* values of Ω_{m0}; the value of Ω_{m0} is essentially insensitive to the value f_{vi}.

unrealistically small values of Ω_{m0}, an issue we will discuss further in Sec. 4.3. Given probability distributions such as these that are significantly skewed relative to a Gaussian distribution, a more typical estimate of any parameter θ is given by the expectation value $\langle\theta\rangle = \int_{-\infty}^{+\infty} \theta\, w(\theta)\, d\theta$, where $w(\theta)$ is the normalised weight. While the bestfit value gives the most probable individual parameters, the expectation value is the average one would obtain given many measurements of the parameter in many universes. In Table 1 we have displayed the expectation values of Ω_{m0} and f_{v0}, together with the bestfit value of Ω_{m0} for comparison. In the cases in which the bestfit value of Ω_{m0} takes the smallest values, namely the Constitution, SALT2 and MLCS31 samples of Hicken et al. (2009) and the Union2 sample of Amanullah et al. (2010), the bestfit value of Ω_{m0} differs from the expectation value by a factor close to one standard deviation.

The extremely small bestfit values of Ω_{m0} for the Union and Constitution samples — or equivalently the unusually large values of f_{v0} — match those found by Kwan et al. (2009), which led these researchers to draw unfavourable conclusions about the TS model. However, Kwan et al. reasoned that this was due to inclusion of extra data in the Union and Constitution samples, as compared to the Riess07 sample. In particular, there are a larger number of SNe Ia in the redshift range $0.35 < z < 0.4$ in the Union sample, and in the range $0 < z < 0.2$ in the Constitution sample. While the inclusion of SNe Ia at extremely close distances below the scale of statistical homogeneity $z < 0.033$ is a separate systematic issue that needs to be carefully investigated, the results of the MLCS2k2–reduced samples in Table 1 refute the claim of Kwan et al. (2009) that it is the greater sample size that is the main issue[12]. The parameters of the TS model are not sensitive to small changes in the SNe Ia data, as Kwan et al. maintain. Rather, we see that the primary question is the method of data reduction. While the MLCS31 sample, fit with $R_V = 3.1$ produces results close to the SALT/SALT II fits, the MLCS17 sample, with the largest number of SNe Ia fit by the MLCS2k2 method, yields a bestfit value $\Omega_{m0} = 0.20^{+0.10}_{-0.17}$, and the SDSS-II sample of Kessler et al. (2009) a bestfit value of $\Omega_{m0} = 0.40^{+0.09}_{-0.11}$. The parameters found from the MLCS17 and SDSS-II samples agree with those of the Riess07 Gold sample to within one standard deviation.

We conclude that the MLCS-reduced SN Ia samples, with appropriate treatment of host galaxy reddening, provide a better fit to the TS model than the SALT–reduced samples. We will see in Sec. 4.3 that this carries through to the Bayesian statistical evidence as well. Our results there-

---

[12] Among other general statements Kwan et al. (2009) make a particular comment: "The best-fitting parameters of the FB model are extremely sensitive to small changes in the SNe Ia data as it needs to compensate for these by a large variation in f_{vi} when fitted to an another redshift distribution with a different amount of error on each SNe Ia. In addition, there is a special set of values for f_{vi} which will mimic ΛCDM parameters well, ..." These statements – together with other statements about the role of the initial void fraction, f_{vi} – are erroneous, since as we have already observed the values of Ω_{m0} and f_{v0} are insensitive to the value of f_{vi}. Kwan et al. (2009) appear to have not understood the quantitative role of this parameter in the general exact solution (Wiltshire 2007b).

Table 3. Expectation values for the parameters of the timescape model from SALT-reduced SN Ia data, recomputed with the timescape model luminosity distance. Distance normalisation is arbitrary. The bestfit value of Ω_{m0} is in brackets.

Dataset	N	χ^2	Ω_{m0}	f_{v0}
Union (TS)	307	350.6	$0.13^{+0.10}_{-0.08}(0.09)$	$0.91^{+0.07}_{-0.06}$
Union (ΛCDM)		344.1	$0.28^{+0.03}_{-0.03}(0.28)$	
Const. (TS)	397	319.7	$0.13^{+0.09}_{-0.08}(0.08)$	$0.91^{+0.06}_{-0.06}$
Const. (ΛCDM)		312.9	$0.29^{+0.03}_{-0.03}(0.28)$	

fore support the observation of Sollerman et al. (2009), who find that for the SDSS-II supernovae of Kessler et al. (2009) reduced with the MLCS2k2 fitter, nonstandard cosmological models can provide a better fit to the data than the ΛCDM model.

4.2 Recalibrating the SALT SNe Ia

Having established that the primary issue for the goodness of fit of the TS model relative to the ΛCDM model is the data reduction method used, we should examine the extent to which implicit use of the ΛCDM model in data calibration affects the SALT/SALT II samples. It is difficult to assess all the ways in which the assumption of a homogeneous cosmology is built into the SALT data reduction procedure. However, it is relatively straightforward to adapt the `simple_cosfitter` code, which implements the SALT procedure, to use the luminosity distance of other cosmological models.

We replaced the module of `simple_cosfitter` that implements the spatially flat ΛCDM luminosity distance by one that computes the TS luminosity distance (14). Leaving the rest of the `simple_cosfitter` code unchanged, we reran the parameter fits. This amounts to taking the published stretch and colour parameters for each supernova, and recomputing Ω_{m0} along with the empirical parameters $\mathcal{M}$, α and β of eq. (22).

The values of Ω_{m0} and the minimum χ^2 that result from this reanalysis are displayed in Table 3. Since the comparable published values for the ΛCDM model often include BAO or WMAP priors, we also show the corresponding parameter values we obtained ourselves using `simple_cosfitter` applied to the spatially flat ΛCDM model. The results indicate that the expectation values of Ω_{m0} increase only very slightly from the values of Table 1. However, the bestfit value of Ω_{m0} is much closer to the expectation value for the Constitution sample. The parameters α, β, and M_B (calculated from $\mathcal{M}$ with[13] $H_0 = 65$ km s^{-1} Mpc^{-1}) are shown in Table 4. Both the TS and `simple_cosfitter` results are well within the uncertainties quoted in Hicken et al. (2009). Given that the Constitution set contains the Union set, it is not surprising that their corresponding Ω_{m0} values should be the same, when calculated for each model, as Table 3 shows. The addition of the new CfA3 SNe Ia to the Union sample
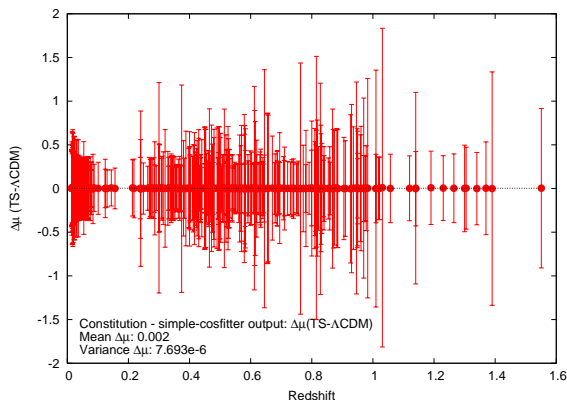
---

[13] We will simply adopt the same Hubble constant normalization as Hicken et al. (2009), who took this value.

Table 4. Values for the global parameters from SALT-reduced SN Ia data, computed by `simple_cosfitter` with the ΛCDM and TS luminosity distances.

Dataset	α	β	M_B
Union (TS)	$1.32^{+0.12}_{-0.12}$	$2.37^{+0.12}_{-0.12}$	-19.42
Union (ΛCDM)[1]	$1.33^{+0.12}_{-0.12}$	$2.38^{+0.13}_{-0.12}$	-19.46
Const. (TS)	$1.29^{+0.10}_{-0.10}$	$2.49^{+0.11}_{-0.11}$	-19.43
Const. (ΛCDM)[2]	$1.31^{+0.10}_{-0.10}$	$2.50^{+0.11}_{-0.11}$	-19.46

[1] Kowalski et al. (2008) values: $\alpha = 1.24^{+0.10}_{-0.10}$, $\beta = 2.28^{+0.11}_{-0.11}$.
[2] Hicken et al. (2009) values: $\alpha = 1.34^{+0.08}_{-0.08}$, $\beta = 2.59^{+0.12}_{-0.08}$, $M_B = -19.46$ with $H_0 = 65$ km s^{-1} Mpc^{-1} .

Figure 5. Differences in the distance moduli obtained by a SALT fit to the Constitution sample using the `simple_cosfitter` code adapted to: (i) the spatially flat ΛCDM model, and, alternatively, (ii) the TS model; as a function of redshift.

Table 5. Expectation values of Ω_{m0} (with bestfit values in brackets), for the 140 SNe Ia common to the Riess07 Gold (R), Union (U), and Constitution (C) samples. For the Union and Constitution subsamples the results of fits to the published data (p); and to `simple_cosfitter` fit data (f), are both shown. Bayes factors, with priors $0.01 \leqslant \Omega_{m0} \leqslant 0.95$ (and $55 \leqslant H_0 \leqslant 75$ km sec^{-1} Mpc^{-1} where relevant), for the TS model relative to the spatially flat ΛCDM model are also given.

Dataset	Ω_{m0}	f_{v0}	$\ln B$
R140	$0.33^{+0.15}_{-0.14}(0.36)$	$0.76^{+0.13}_{-0.13}$	0.14
U140(p)	$0.21^{+0.17}_{-0.20}(0.23)$	$0.85^{+0.14}_{-0.13}$	0.43
U140(f)	$0.16^{+0.12}_{-0.10}(0.13)$	$0.89^{+0.07}_{-0.09}$	0.14
C140(p)	$0.17^{+0.16}_{-0.16}(0.17)$	$0.88^{+0.11}_{-0.12}$	0.56
C140(f)	$0.18^{+0.12}_{-0.12}(0.17)$	$0.87^{+0.09}_{-0.09}$	0.17

changes the fits of the global parameters α, β, and $\mathcal{M}$, and consequently the estimate of Ω_{m0}, but Table 4 shows these changes are relatively small.

Overall the differences between Table 1 and Table 3 are relatively small. In particular, whether or not the ΛCDM or TS luminosity distance is assumed, the SALT-reduced data still produces consistently higher fits to the present epoch void fraction, f_{v0}, than that of the MLCS-reduced samples (other than MLCS31). The resulting Ω_{m0} values depend only very weakly on whether the luminosity distance assumed by the SALT fitter is a TS one or a ΛCDM one. Furthermore, the distance moduli themselves show insignificant differences: the difference between the two measures is plotted in Fig. 5 (on the same scale as used in Figs. 1 and 2 for comparison).

Fig. 5 demonstrates that use of the TS luminosity distance is capable of reproducing the SALT ΛCDM results to great precision. Thus the differences in the expectation values of cosmological parameters found in Table 1 between the MLCS and SALT fitters must be a consequence of systematic differences, rather than the luminosity distance relation assumed by SALT.

As a check that the differences between the fitters are not simply a consequence of the inclusion of different SNe Ia subsamples, we have compared the cosmological parameters

determined from the subsample of 140 SNe Ia common to the Riess07 Gold, Union, and Constitution datasets, which was used in generating Figs. 1 and 2. In Table 5 we show the TS cosmological parameters determined using the both the published data for the Riess07 dataset[14], Union and Constitution samples, and also our own SALT fit (with the TS luminosity distance) of these 140 points alone. We see that the subsets of published data values produce higher estimates of Ω_{m0} for each sample than each of the complete sets given in Table 1, and that the greatest percentage increase is for the Constitution sample. Furthermore, a `simple_cosfitter` fit to the subsample of 140 SNe Ia alone also produces higher estimates of Ω_{m0}, which differ somewhat from the subsample of the published values only in the case of the Union sample. However, in all cases the SALT–reduced Union and Constitution subsamples still have a significantly lower value of Ω_{m0} than the MLCS reduced Riess07 subsample. Consequently, intrinsic differences in the MLCS and SALT methods appear to be the dominating cause of the variance in cosmological parameter estimates for the TS model.

The Bayes factors, representing the integrated likelihood of the TS model over that of the spatially flat ΛCDM model have also been given in Table 5. By the Jeffreys scale (Trotta 2008) these results indicate that the models are statistically indistinguishable for the subsample of 140 SNe Ia, regardless of the fitter used. For the Riess07 Gold data this is interesting, given that the whole sample of 182 SNe Ia gives $\ln B = -1.20$ with mild positive evidence in favour of the ΛCDM model. Although the inclusion of the additional 42 SNe Ia in the Riess07 Gold sample does not greatly affect the values of cosmological parameters, it significantly changes the relative goodness of fit of the TS and ΛCDM models. Since the Constitution sample simply augments the

---

[14] For the subsample of 140 SNe Ia from Riess07 gold dataset a fit of the Hubble constant gives $H_0 = (61.4^{+1.4}_{-1.5}, 62.3^{+1.4}_{-1.8})$ km sec^{-1} Mpc^{-1} for the TS and spatially flat ΛCDM models respectively as compared to the respective values $H_0 = (61.7^{+1.2}_{-1.1}, 62.6 \pm 1.3)$ km sec^{-1} Mpc^{-1} for the full sample of 182 SNe Ia. As remarked in Sec. 3.4 this is not an absolute determination of H_0, as the data assumes an overall calibration; but relatively speaking, the favoured value of H_0 is only very slightly reduced by restricting to the subsample.

Union sample with more recent data, the reason for the exclusion of the 42 SNe Ia in question boils down to the differences in the selection cuts of Kowalski et al. (2008) as compared to those of Riess et al. (2007).

4.3 The Statistical Homogeneity Scale

There are a huge number of potential sources of systematic errors, which, treated differently in the MLCS and SALT fitters, might be responsible for the differences in parameter estimates obtained for the TS model. As we have already discussed in Sec. 3.3.1, in the TS model an average Hubble flow is only expected on scales greater than the statistical homogeneity scale[15] (SHS). Thus for consistency, in performing any parameter fits on the TS model, a cut should be applied to data at redshifts below the SHS.

For the SALT datasets the inclusion of significant numbers of SNe Ia below the SHS could conceivably bias the global fits of α, β, $\mathcal{M}$ and Ω_{m0}. The potential impact of the SHS on the MLCS datasets is less clear, as the fitter is trained using a set of nearby SNe Ia that are far enough into the Hubble flow for peculiar velocities to be negligible, yet still close enough for the linear Hubble law to hold (Jha et al. 2007). In practise, the training set includes some SNe Ia within the SHS, so there may be systematic issues associated with the SHS, just much more subtle.

As a first check on whether the discrepancy between the values of Ω_{m0} determined by the SALT and MLCS methods can be accounted for by making cuts at the SHS scale, we have determined parameters for fits to the TS model with cuts made: (i) by excluding objects at redshifts $z < 0.024$, which corresponds to the $H_0 d_{SN} \simeq 7400 \, \mathrm{km \, sec^{-1}}$ Hubble bubble partition assumed by Jha et al. (2007); Riess et al. (2007) and Hicken et al. (2009)); and (ii) by excluding objects with redshifts $z < 0.033$, corresponding to the estimated scale of statistical homogeneity, $100/h$ Mpc. The resulting values of Ω_{m0} are compared with the values obtained from the full dataset in Table 6. Bayes factors for a fit of the TS model relative to the spatially flat ΛCDM model are also displayed.

In all cases the relevant cuts lead to somewhat larger values of Ω_{m0}, with the exception of the subsample of 140 SNe Ia from the Riess07 Gold dataset, which was discussed in Table 5. In the SALT cases the increase in the expectation value of Ω_{m0} is not particularly large. However, the bestfit value of Ω_{m0} increases generally by a factor of three from the full sample to the SHS cut sample. Since the bestfit value of Ω_{m0} is much closer to the expectation value for the SALT samples once SHS cuts are made, it shows that the fits are no longer so strongly skewed away from being Gaussian with bestfit values of Ω_{m0} at unreasonably small values. This demonstrates that the main criticism of Kwan et al. (2009) is invalid once the SHS cut is made.

---

[15] We prefer to the terminology "statistical homogeneity scale" to the more commonly used "Hubble bubble" terminology, since the latter is often taken to be a single large local void. In the ΛCDM context, such a feature is, strictly speaking, anomalous. In the TS model an *apparent* Hubble bubble at any typical wall location is an expected for averages below the statistical homogeneity scale, given the dominance of of $30/h$ Mpc diameter voids by volume in the late epoch universe.

Table 6. Parameter values for SN Ia datasets, applying homogeneity scale cuts, the first at the Hubble bubble radius of $z_{min} = 0.024$ (e.g. Jha et al. (2007)), the second at $z_{min} = 0.033$, corresponding to the scale of statistical homogeneity estimated to be $\sim 100 \, h^{-1}$ Mpc. Expectation values of Ω_{m0} are shown, with bestfit values in brackets. For the SALT/SALT–II fits (Union, Constitution, SALT2, Union2) the parameters have been recomputed by adapting `simple_cosfitter` to the TS model in each case.

Dataset	z cut	N	χ^2	Ω_{m0}	ln B
Gold	$\geqslant 0.024$	182	162.7	$0.30^{+0.14}_{-0.13}(0.33)$	-1.20
	$\geqslant 0.033$	169	151.8	$0.31^{+0.15}_{-0.13}(0.34)$	-1.18
R140	$\geqslant 0.024$	140	102.7	$0.33^{+0.16}_{-0.14}(0.36)$	0.14
	$\geqslant 0.033$	132	96.2	$0.26^{+0.20}_{-0.25}(0.30)$	0.78
MLCS17	None	372	401.7	$0.18^{+0.13}_{-0.15}(0.20)$	0.77
	$\geqslant 0.024$	282	315.7	$0.17^{+0.13}_{-0.16}(0.19)$	0.37
	$\geqslant 0.033$	234	260.2	$0.19^{+0.14}_{-0.17}(0.21)$	0.57
MLCS31	None	366	429.5	$0.07^{+0.05}_{-0.06}(0.01)$	-1.57
	$\geqslant 0.024$	278	332.2	$0.09^{+0.08}_{-0.08}(0.01)$	0.13
	$\geqslant 0.033$	229	263.3	$0.11^{+0.11}_{-0.10}(0.03)$	1.09
SDSS-II	None	288	240.8	$0.39^{+0.11}_{-0.09}(0.40)$	0.09
	$\geqslant 0.024$	284	238.4	$0.40^{+0.11}_{-0.10}(0.41)$	0.27
	$\geqslant 0.033$	272	214.5	$0.42^{+0.10}_{-0.10}(0.44)$	0.53
Union	None	307	350.6	$0.13^{+0.10}_{-0.08}(0.07)$	-2.04
	$\geqslant 0.024$	288	333.4	$0.15^{+0.10}_{-0.09}(0.14)$	-1.53
	$\geqslant 0.033$	275	318.0	$0.18^{+0.11}_{-0.11}(0.20)$	-0.86
Const.	None	397	319.6	$0.13^{+0.09}_{-0.08}(0.06)$	-1.54
	$\geqslant 0.024$	351	293.8	$0.13^{+0.09}_{-0.08}(0.09)$	-1.57
	$\geqslant 0.033$	309	275.9	$0.16^{+0.10}_{-0.10}(0.15)$	-1.06
SALT2	None	351	402.5	$0.10^{+0.08}_{-0.06}(0.02)$	-2.25
	$\geqslant 0.024$	278	342.1	$0.11^{+0.08}_{-0.06}(0.03)$	-2.22
	$\geqslant 0.033$	235	305.5	$0.13^{+0.09}_{-0.07}(0.09)$	-1.55
Union2	None	557	520.3	$0.09^{+0.07}_{-0.08}(0.05)$	-2.65
	$\geqslant 0.024$	504	483.5	$0.10^{+0.08}_{-0.06}(0.09)$	-2.25
	$\geqslant 0.033$	457	428.4	$0.10^{+0.08}_{-0.06}(0.15)$	-3.46
CSP	None	56	62.3	$0.11^{+0.08}_{-0.10}(0.01)$	-4.23
	$\geqslant 0.024$	47	69.1	$0.12^{+0.13}_{-0.11}(0.01)$	-4.03
	$\geqslant 0.033$	43	46.0	$0.13^{+0.12}_{-0.12}(0.01)$	-3.34

In all the MLCS2k2 cases, the Bayes factor improves in favour of the TS model with the redshift cuts, but the improvement is weak and, with the exception of MLCS31, generally not enough to statistically distinguish the models. For the SALT reduced data, by contrast, the data generally indicate mild positive evidence against the TS model on the Jeffreys scale (Trotta 2008). For all SALT datasets apart

Figure 6. Bestfit values (solid line) and expectation values (dotted line) of Ω_{m0} for successive redshift cuts for eight SNe Ia samples. The probability distributions for SALT Ω_{m0} fits (left column) make a transition from negative skew to positive skew, while those MLCS samples (right column) which already provide better fits to the TS model are always positively skewed.
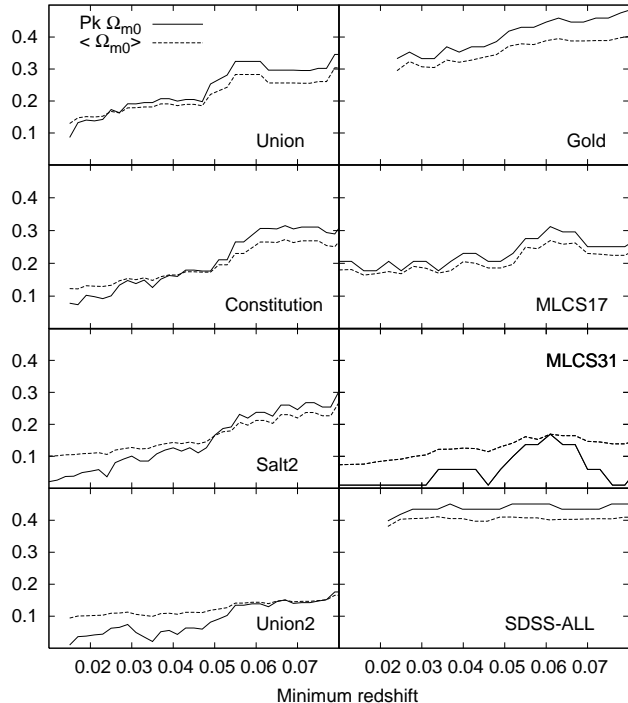
from Union2 the Bayesian evidence in favour of the ΛCDM model is weaker once the SHS cut is applied.

In order to further test the issue of redshift cuts, we have repeated our analysis by applying a cut at redshifts which range from the minimum value in each dataset up to $z_{min} = 0.08$. The results are shown in Figs. 6 and Figs. 7. The Bayes factor for the SHS ($z_{min} = 0.033$) cut on the Union2 sample turns out to mark the beginning of a downward trough in an otherwise increasing trend.

Fig. 6 provides a direct demonstration of how excluding the SNe Ia below the SHS leads to to a better agreement between the bestfit and expectation values of Ω_{m0} in the SALT/SALT II reduced datasets. In fact, it also reveals differences between the SALT and SALT II fitters. For the Union and Constitution datasets, reduced by SALT, we see that below the SHS the bestfit value is below the expectation value, i.e., negatively skewed. For cuts in the range $0.03 \lesssim z_{min} \lesssim 0.05$ the bestfit and expectation values of Ω_{m0} are roughly comparable for these samples, while for $z_{min} \gtrsim 0.05$ the bestfit value is positively skewed. For SALT2 and Union2, reduced by SALT II, the bestfit value remains negatively skewed for cuts up to $z_{min} \lesssim 0.055$.

In the case of the datasets that the TS model fits well – Riess07 Gold, MLCS17 and SDSS-II – the skew is always positive, i.e., the bestfit value is greater than the expectation value. The skew is larger for the cuts at higher redshifts, par-

ticularly for the Gold and SDSS-II samples. For MLCS31, the bestfit value is negatively skewed, and the fit is generally poor, in the sense that this peak probability is very significantly skewed.

These results suggest that the way that the SALT fitters treat nearby objects – the inclusion of large numbers of them as well as the treatment of their color variations and host galaxy dust – does affect the TS cosmology fits.

Finally, for completeness we have added the recently published first dataset from the Carnegie Supernova Project (CSP) (Freedman et al. 2009) to Table 6. This is a much smaller dataset than the others. The CSP differs from other projects by working in the near infrared, and consequently the data is differently reduced. However, in analysing their data Freedman et al. (2009) have adopted a reduced–$\chi^2 = 1$ approach, conceptually similar to the approaches used in the SALT/SALT-II fits. Nuisance parameters, including R_V, are determined by minimising Hubble residuals for the whole diagram. In Table 6 we have only presented fits to the TS model for the "out of the box" data of Freedman et al. (2009), which was fit to a FLRW model with constant dark energy equation of state parameter, w. To be more confident about the conclusions we should redo the data reduction for the TS model. However, such a task requires considerable effort, and we will defer this until such a time as significantly more data is available. At this stage we note that Freedman et al. (2009) found a value of $R_V = 1.74 \pm 0.27\,(\text{stat}) \pm 0.01\,(\text{sys})$, considerably lower than the Milky Way $R_V = 3.1$ value, which is consistent with the values of the corresponding values of β typical in the SALT/SALT-II fits. Furthermore, the very low expectation values of Ω_{m0} are most consistent with SALT2 and Union2. While the bestfit value of Ω_{m0} is essentially driven to zero, giving an extremely skewed distribution, we must recall that this was also the case for Union2 "out of the box" data in Table 1 before the SALT-II parameters were recomputed for the TS luminosity distance. Given the similarity in approach, we would expect an improvement in the bestfit values if the TS luminosity distance was assumed in the data reduction.

4.4 Systematic issues for MLCS

The erratic results from MLCS31 ($R_V = 3.1$) for the minimum redshift cuts in Figs. 6 and Figs. 7, and the relatively stable results from MLCS17 ($R_V = 1.7$) and SDSS-II ($R_V = 2.18$) suggest that while the MLCS samples are better fit by the TS model, such fits are still highly affected by the treatment of dust extinction and reddening. However, the issues are much subtler than simply the value of R_V assumed. In particular, the Riess07 gold dataset (Riess et al. 2007) and the MLCS31 dataset (Hicken et al. 2009) are both fit with $R_V = 3.1$ and yet they produce expectation values of Ω_{m0} which differ by a factor of three, once the SHS cut is made. Similarly, the MLCS17 dataset (Hicken et al. 2009) and SDSS-II dataset are both fit with low R_V values, respectively 1.7 and 2.18, while producing expectation values of Ω_{m0} which differ by a factor of two, for the SHS-cut samples.

These large differences in the probable values of Ω_{m0} suggest that the different assumptions in sample selection made with different versions of MLCS2k2 have a very signif-

Figure 7. Bayesian evidence: $\ln B$ for the TS model relative to the spatially flat ΛCDMmodel for successive redshift cuts for nine SNe Ia samples. The SALT/SALT II reduced sets are in the left panel, the MLCS2k2 reduced samples in the right panel.
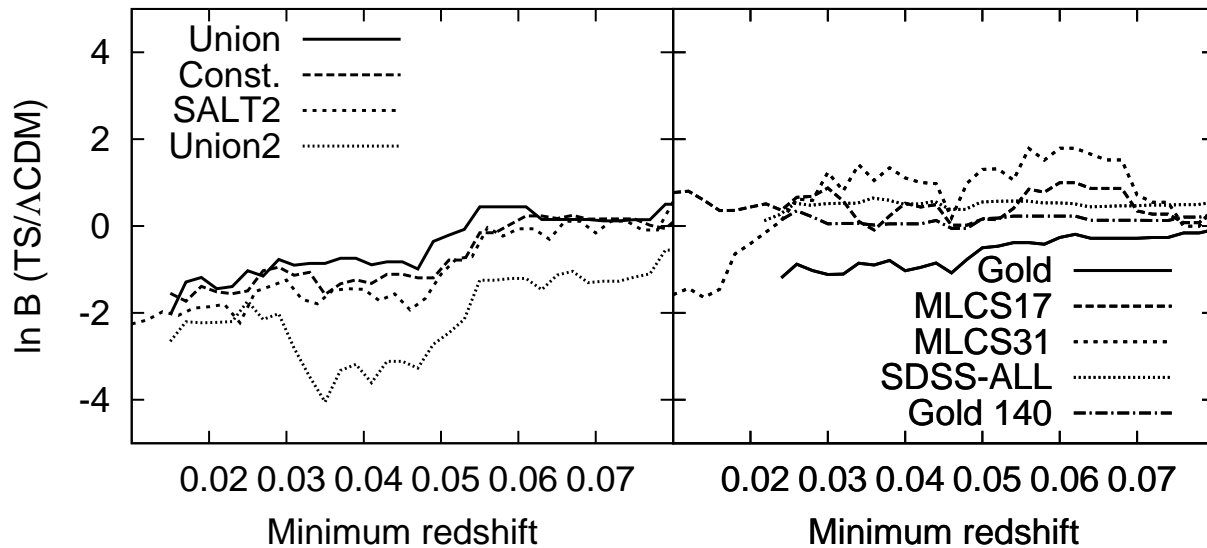
icant impact in the determination of TS model parameters. As a check, we have redone the analysis of Table 6 for the following samples: Sample A of the 76 SNe Ia common to the Riess07 Gold and MLCS31 datasets; and Sample B of the 74 SNe Ia common to the Riess07 Gold and MLCS17 datasets. The two samples include the same SNe Ia apart from four objects – three SNe Ia, SN 1999gp at $z = 0.026$, SN 1991U at $z = 0.033$, and SN 1992J at $z = 0.046$ are in Gold and MLCS31 but not in MLCS17, and one, SN 2004D4dw at $z = 0.961$, is in Gold and MLCS17 but not in MLCS31. We have tested the both samples in full, and with a SHS cut. Of the four SNe Ia not common to both Sample A and Sample B, only one, SN 1999gp is below the SHS, though SN 1991U at $z = 0.033$ is borderline. In addition, we make a final cut to include the 66 SNe Ia above the SHS which are common to both samples.

From Table 7 we see that the expected and bestfit values of Ω_{m0} for the Riess07 Gold sample are somewhat reduced relative to those of the full sample given in Table 7, and that they agree with the corresponding values for the MLCS31 and MLCS17 subsamples within the 1σ uncertainties. Nonetheless there are still some differences in the central expectation values, particularly in the case of the MLCS31 sample. Since the Gold and MLCS31 samples assume the same $R_V = 3.1$, the differences might be a consequence of the different assumptions about extinction priors (Jha et al. 2007) made in the different implementations of MLCS2k2.

While in most cases the Bayesian evidence for the TS model relative to the spatially flat ΛCDM model is improved for the subsamples of Table 7, the most striking change comes about when the MLCS17-excluded SNe Ia SN 1991U and SN 1992J are excluded from the SHS–cut Gold and MLCS31 A samples, reducing these from 68 to 66 objects. The effect of this is to substantially increase Ω_{m0} in both cases, to remove a dramatic negative skew of the bestfit Ω_{m0} in the Gold subsample, and to change the Bayesian evidence by an order of magnitude, (a factor 3 in B), in the

Table 7. Parameter values for SN Ia datasets, applying homogeneity scale cuts, to the 76 SNe Ia common to Riess07 Gold and MLCS31 (Sample A); and to the 74 SNe Ia common to Riess07 Gold and MLCS17 (Sample B).

Dataset	z cut	N	χ^2	Ω_{m0}	$\ln B$
A Gold	$\geqslant 0.024$	76	60.7	$0.20^{+0.20}_{-0.19}(0.13)$	0.73
	$\geqslant 0.033$	68	51.0	$0.19^{+0.19}_{-0.18}(0.02)$	0.41
	$\geqslant 0.033$	66	41.3	$0.23^{+0.24}_{-0.22}(0.23)$	0.84
A MLCS31	$\geqslant 0.024$	76	76.6	$0.14^{+0.13}_{-0.13}(0.01)$	0.09
	$\geqslant 0.033$	68	65.7	$0.13^{+0.11}_{-0.12}(0.01)$	-0.73
	$\geqslant 0.033$	66	51.9	$0.16^{+0.16}_{-0.15}(0.01)$	0.40
B Gold	$\geqslant 0.024$	74	50.5	$0.24^{+0.23}_{-0.23}(0.26)$	0.80
	$\geqslant 0.033$	67	41.3	$0.23^{+0.23}_{-0.22}(0.23)$	0.93
B MLCS17	$\geqslant 0.024$	76	76.2	$0.18^{+0.20}_{-0.17}(0.11)$	0.93
	$\geqslant 0.033$	67	74.5	$0.18^{+0.19}_{-0.17}(0.01)$	0.86

case of the MLCS31 subsample. We have not investigated the reasons for the exclusion of SN 1991U and SN 1992J in the MLCS17 sample; however, they do indeed appear to be outliers in the present analysis. To test this hypothesis, we have recomputed the Riess07 Gold and MLCS31 entries of Table 6 with the three MLCS17-excluded SNe Ia removed. The effect of removing two SNe Ia on these larger samples might expected to be less. Nonetheless, the SHS-cut samples do show a dramatic change. The Bayesian evidence for the TS model is significantly increased in each case.

Finally, given that individual SNe Ia which were excluded from either the MLCS17 or MLCS31 samples by Hicken et al. (2009) are potential outliers, (at least for the ΛCDM model), we recompute Table 6 for the 352 SNe Ia

Table 8. Recalculation of Table 6 for the Riess et al. (2007) Gold sample and the Hicken et al. (2009) MLCS31 samples, with three low redshift SNe Ia that were excluded by Hicken et al. (2009) from their MLCS17 sample, SN 1991U, SN 1992J and SN 1999gp, excluded.

Dataset	z cut	N	χ^2	Ω_{m0}	$\ln B$
Gold	$\geqslant 0.024$	179	151.0	$0.34^{+0.13}_{-0.11}(0.36)$	-0.77
	$\geqslant 0.033$	167	139.9	$0.31^{+0.15}_{-0.13}(0.34)$	-0.63
MLCS31	None	363	414.9	$0.08^{+0.05}_{-0.07}(0.01)$	-1.27
	$\geqslant 0.024$	276	317.2	$0.10^{+0.08}_{-0.09}(0.01)$	0.50
	$\geqslant 0.033$	227	248.4	$0.13^{+0.13}_{-0.12}(0.08)$	1.68

Table 9. Recalculation of Table 6 for the 352 SNe Ia common to both the MLCS31 and MLCS17 samples of Hicken et al. (2009).

Dataset	z cut	N	χ^2	Ω_{m0}	$\ln B$
MLCS17	None	352	366.9	$0.16^{+0.13}_{-0.15}(0.17)$	1.20
	$\geqslant 0.024$	266	293.8	$0.16^{+0.14}_{-0.15}(0.18)$	1.10
	$\geqslant 0.033$	219	238.1	$0.19^{+0.14}_{-0.18}(0.21)$	1.37
MLCS31	None	352	403.4	$0.08^{+0.05}_{-0.07}(0.01)$	-1.31
	$\geqslant 0.024$	266	310.0	$0.09^{+0.09}_{-0.08}(0.01)$	0.39
	$\geqslant 0.033$	219	242.1	$0.12^{+0.12}_{-0.11}(0.07)$	1.55

common to both MLCS31 and MLCS17 samples, using each R_V normalization. The results are shown in Table 9. For the SHS-cut samples, there is no overall change to the Ω_{m0} parameter for the MLCS17 sample, but the bestfit value of MLCS31 sample is increased to be more in line with the Table 8 result. There is now positive Bayesian evidence for the TS model versus the spatially flat ΛCDM model for MLCS17 as well as MLCS31 with the SHS cut.

While the analysis of this section has not been able to resolve the issue of how similar R_V values can lead to quite different expectation values of Ω_{m0}, as evidenced by the Riess07 Gold sample versus the MLCS31 sample, or by the SDSS-II sample versus the MLCS17 sample, it does show that the question of extinction priors, and the SNe Ia excluded by particular priors, may be crucial to this. Ideally one should re-evaluate the MLCS2k2 parameter fitting using the TS model at the outset.

4.5 Parameter sensitivity in the timescape model

The parameter Ω_{m0} is much more sensitive to the method of data reduction in the case of the TS model than is the case for the ΛCDM model. Of course, we have not explored the goodness of fit of the ΛCDM model when cuts are made at the SHS in the same way that we have for the TS model, as there is no theoretical rationale for doing so.

In order to understand differences in the degree of sensitivity of parameter estimation between the two models, let us consider the fit of the MLCS2k2 data once a SHS cut is

Figure 8. Confidence limits for the TS model fits to $z \geqslant 0.033$ cut samples of Gold07 (Table 8), SDSS-II (Table 6), MLCS17 and MLCS31 (Table 9). In each case an overall normalization of the Hubble constant from the published dataset is assumed.
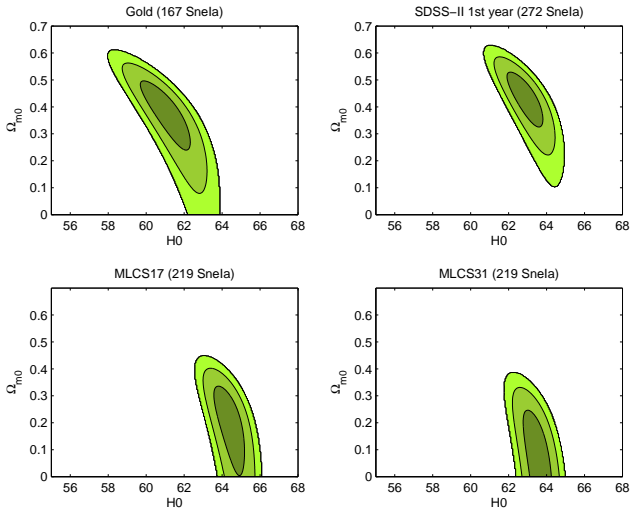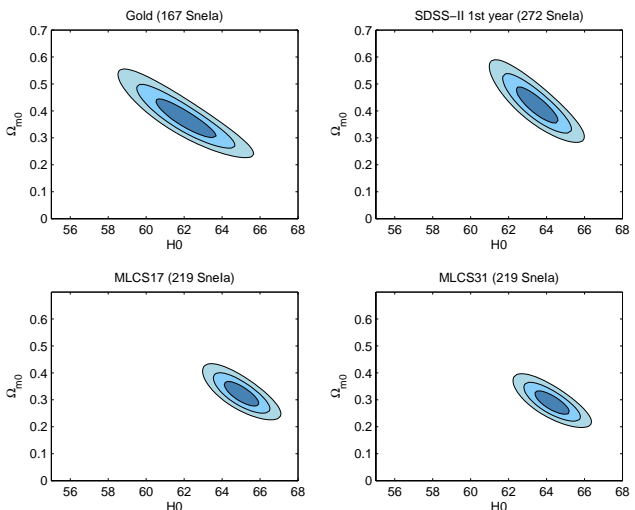

Figure 9. Confidence limits for the ΛCDM model fits to $z \geqslant 0.033$ cut samples of Gold07 (Table 8), SDSS-II (Table 6), MLCS17 and MLCS31 (Table 9). In each case an overall normalization of the Hubble constant from the published dataset is assumed.

made. In Fig. 8 we display confidence contours for the SHS ($z \geqslant 0.033$) cut Gold sample of Table 8, the SDSS-II sample of Table 6, and the MLCS17 and MLCS31 samples of Table 9. (In all cases SNe Ia events excluded from either the MLCS17 or MLCS31 samples have been cut.) Corresponding plots for the spatially flat ΛCDM model are shown in Fig. 9. Equivalent contour plots for SALT-reduced samples are not shown, since the value of H_0 is marginalised over in the SALT data reduction process.

Clearly there are some differences which are intrinsic to the data reduction method, since even in the ΛCDM model the best fit value of the matter density parameter varies from 0.40 ± 0.04 for the SDSS-II sample to 0.26 ± 0.03 for

the MLCS31 sample. The fact that the dressed matter density parameter of the TS model is more sensitive than the corresponding value of Ω_{m0} for the ΛCDM model is essentially a consequence of different manner in which the parameters Ω_{m0} and H_0 affect the luminosity distances in the two models. In the case of the ΛCDM model the confidence contours are at roughly $45°$ for the scale chosen in Fig. 9. By contrast, although the area of the contours is comparable in both models, on the same scale the confidence contours for the TS model are close to vertical, especially for the smaller values of $\Omega_{m0} \sim 0.3$. Thus in the case of the TS model the parameter H_0 is more tightly constrained than in the ΛCDM model, given whatever overall normalization of absolute magnitudes is assumed in the data, while the parameter Ω_{m0} is less constrained.

Physically, these differences can be understood to be a consequence of the fact that on one hand the ΛCDM model has actual accelerating expansion, whereas the apparent acceleration in the TS model is less pronounced and its luminosity distance is closer to that of an empty Milne universe.

5   DISCUSSION

Even with a SHS cut there remain considerable systematic issues – probably concerning extinction and reddening by dust, and intrinsic SNe Ia colour variations – which need to be resolved before one can draw any reliable conclusions about the goodness of fit of one cosmological model over another. These issues have been discussed by many other groups – see, e.g., Hicken et al. (2009); Freedman et al. (2009); Kessler et al. (2009); Sullivan et al. (2010); Lampeitl et al. (2010).

5.1   Reddening by dust

There are at least four possible sources of dust: (i) dust in the Milky Way; (ii) dust in the host galaxy; (iii) dust in the local circumstellar environment of the supernova event; and (iv) dust in the intergalactic medium. Whereas Milky way dust, with the reddening law $R_V = 3.1$ is well understood, we do not have direct a priori knowledge of the other three possible sources of dust. The present status of our understanding is that while there appears to be no direct evidence of an intergalactic gray dust which would significantly alter the SNe Ia luminosity distance relations, the situation regarding dust within the host galaxy, and within the supernova local environment, is a complex one.

5.1.1   Host galaxy dust

The nature of dust in the host galaxy would appear to be the most significant systematic unknown, given that assuming different values of R_V can lead to substantial differences in the MLCS2k2 fitters, and similarly for the value of β in the SALT/SALT-II fitters. Superficially, the results of Table 9 might appear to favour the MLCS17 over the MLCS31 sample for the TS model, given the lower value of χ^2. However, it is noticeable that the results for the MLCS17 sample show essentially no change with the cuts made up to the SHS. By contrast, the Bayesian evidence for the TS model over the

spatially flat ΛCDM model shows a marked improvement in Tables 8 and 9 when the SHS cut is applied.

For consistency of the TS scenario an apparent Hubble bubble feature should be seen below the SHS. Consequently the most likely expectation for reddening and extinction by dust consistent with the above results is that, *at least at low redshifts*, the reddening law for dust in other galaxies is close to the $R_V = 3.1$ law of the Milky Way. Independent support for such a conclusion is provided by the recent studies of Finkelman et al. (2008, 2010) and Folatelli et al. (2010) (CSP).

Finkelman et al. (2008, 2010) studied dust lanes in 15 E/S0 galaxies with $z < 0.033$, and determined extinction properties by fitting model galaxies to the unextinguished parts of the images in each of six spectral bands, and then subtracting these from the actual images. They found an average value $R_V = 2.82 \pm 0.38$ for 8 galaxies in their first study (Finkelman et al. 2008), and $R_V = 2.71 \pm 0.43$ for 7 galaxies in their second investigation (Finkelman et al. 2010). These values are a little lower than the Milky Way value but consistent with it within the uncertainties.

Folatelli et al. (2010) investigated the reddening law properties of SNe Ia in host galaxies at $z < 0.08$ using well-sampled, high-precision optical and near-infrared light curves. Although a value of $R_V \simeq 1.7$ was obtained for the whole sample, once two very highly reddened objects SN 2005A and SN 2006X were excluded, a value of $R_V \simeq 3.2$, similar to the Milky Way one, was obtained by comparison of colour excesses. In contrast to the results obtained by comparison of colour excesses Folatelli et al. (2010) found that fits of absolute magnitude gave $R_V \simeq 1$–2, even when the two highly reddened SNe Ia were excluded. This discrepancy suggests that in addition to the normal interstellar reddening produced in host galaxies, there is an intrinsic dispersion in the colours of normal SNe Ia which is correlated with luminosity but independent of the decline rate. This would suggest that the low R_V values inferred in the MLCS17 and SDSS-II analyses may be anomalous, and furthermore that there may be intrinsic systematic problems with the empirical methodology assumed by the SALT/SALT-II fitters.

5.1.2   Supernova circumstellar dust

The actual picture may be further complicated, however, if the local circumstellar environment of individual SNe Ia is important for a significant subclass of events. That this is potentially the case was borne out by a recent analysis of Wang et al. (2009). They found that within a sample of 158 relatively normal SNe Ia, roughly one third of the objects displayed high photospheric velocities, as determined from Si II $\lambda6355$ absorption lines. The high velocity sample of SNe Ia were found to be on average ~ 0.1 mag redder than the larger group of "normal" supernovae. This high velocity sample includes the two very highly reddened objects SN 2005A and SN 2006X, whose exclusion[16] led to the $R_V \simeq 3.2$

---

[16] Of the events in common to the analysis of Folatelli et al. (2010) and Wang et al. (2009) all apart from three objects SN 2004ef, SN 2005A and SN 2006X are classified by Wang et al. (2009) as "normal". Wang et al. (2009) note that there is no sharp division between their normal and high velocity groupings

estimate of Folatelli et al. (2010). This could either mean that the high velocity sample have intrinsically red $B-V$ colours or that they are associated with dusty local environments. Evidence for the second possibility is directly seen in the case of SN 2006X in the nearby Virgo cluster spiral galaxy[17] M100 (Patat et al. 2007; Wang et al. 2008a,b). A model with multiple scattering of photons by circumstellar dust is found to steepen the effective extinction law (Goobar 2008). Wang et al. (2009) found that their reddened high velocity subsample preferred a lower extinction ratio $R_V \simeq 1.6$ as compared to $R_V \simeq 2.4$ for the normal group, which is consistent with this theoretical model. The difference of the R_V value of the normal group from the corresponding value of Folatelli et al. (2010) may be a further hint of a possible intrinsic colour dispersion of the normal group.

If the sample of Wang et al. (2009) is representative then perhaps of order one third of SNe Ia could have a different effective R_V. We note, for example, that 78 objects are common[18] to the sample of Wang et al. (2009) and the MLCS17 sample (Hicken et al. 2009). Of these 27 are classified as "high velocity" by Wang et al. (2009), and the rest as "normal", which are the same rough proportions as the full sample. However, one must take great care in making generalizations based on low redshift samples, as low redshift SNe Ia are often discovered by targeting galaxies of particular types, such as massive galaxies. This could introduce significant statistical biases as compared to SNe Ia sampled at higher redshifts.

Furthermore, much needs to be done to understand the astrophysics of nonstandard circumstellar dust, as the relative proportion of objects could be affected by evolution. For example, it has been suggested that the nonstandard dust of SN 2006X might be due to circumstellar material accreted from a companion star in the red giant phase (Patat et al. 2007). If the nature of the companion star to a SN Ia

---

when the photospheric velocity approaches a lower value, so that blending can occur to some extent. The object SN 2004ef is the only one treated as normal by Folatelli et al. (2010) while being placed in the high velocity sample by Wang et al. (2009).

[17] The circumstellar material around SN 2006X was identified by the presence of time-variable and blue-shifted Na I D features by Patat et al. (2007), and from a light echo by Wang et al. (2008b). Spectroscopic and photometric analysis of extinction due to circumstellar dust around SN 2006X has been parameterised with $R_V = 1.48 \pm 0.06$ (Wang, Li & Filippenko 2008a). VLT spectropolarimetry (Patat et al. 2009) provides independent confirmation that the intervening dust is different in nature from typical Milky Way dust. SN 2006X is an unusual SN Ia, however, having one of the highest expansion velocities ever observed, as well as being very highly reddened. A further sample of 31 SNe Ia has been studied for the presence of the same Na I D features as SN 2006X by Blondin et al. (2009). The only object in their sample other than SN 2006X which exhibited such features was the highly reddened SN 1999cl, which is classified as a "high velocity" object by Wang et al. (2009). There are 24 objects in common to the studies of Wang et al. (2009) and Blondin et al. (2009) including SN 2006X and SN 1999cl. Of the 22 objects which do not exhibit variable Na I D features, 17 are classed as "normal" by Wang et al. (2009) and 5 as "high velocity". This suggests Na I D variability may not be systematically related to nonstandard dust.

[18] These objects are all at low redshifts, $z < 0.06$, and some 86% are within the SHS.

progenitor is important in characterizing nonstandard dust, then the relative statistics of such events may change with redshift.

5.1.3   Intergalactic dust

The possible cumulative effects of intergalactic dust ejected from galaxies has been investigated by Ménard et al. (2010a), who analysed the reddening of $\sim 85,000$ quasars at $z > 1$ due to the extended halos of 20 million SDSS galaxies at $z \sim 0.3$. They found that on large scales dust extinction has a wavelength dependence described by[19] $R_V \simeq 4.9 \pm 3.2$. The cumulative presence of intergalactic dust along the line of sight turns out not to affect the colour-magnitude-stretch scaling relations, but does bias cosmological parameters in the standard cosmology at a level comparable to current statistical errors, i.e., a few percent (Ménard et al. 2010b). Accounting for the intergalactic dust led to a 6% increase in Ω_{m0} for the spatially flat ΛCDM model. Given the increased sensitivity of Ω_{m0} in the TS model to changes in the treatment of SNe Ia systematics, this bias may have an even greater impact, and should be fully investigated.

5.2   Intrinsic colour variations

As discussed in Sec. 5.1.1 above the analysis of Folatelli et al. (2010) suggests that there may be an intrinsic dispersion in the colours of normal SNe Ia which is correlated with luminosity but independent of the decline rate. This may be significant in understanding the dramatic differences for the TS model between the results of the MLCS2k2 fits and the SALT/SALT–II fits, given that the latter rely on an empirical parameterisation in which the effects of intrinsic colour dispersion are degenerate with those of reddening by dust.

Much effort has gone into both theoretical and observational studies which attempt to find direct correlations between SN Ia luminosity and particular effects, including metallicity of the progenitor, age of the progenitor, asymmetries of the explosion, central density and C/O ratio etc[20]. While these effects could account for further secondary corrections to the light curve fitting which need to be performed to account for intrinsic colour variations, a great many more studies are required to sort out the physics. Indeed, there is a possibility that different effects are involved in a manner which may make them difficult to disentangle as the progenitor population evolves over cosmological time scales.

It is well established that the age of progenitor system is a key variable affecting SNeIa properties, a feature which has been known since the early work of Hamuy et al. (1995), who observed that in their nearby sample, brighter SNeIa tend to occur in late-type galaxies. A broad division of SNe Ia can be made into "prompt" and "delayed" groups (Scannapieco & Bildsten 2005). The former group comprise intrinsically brighter slow-declining SNe Ia which come from a young stellar population and have a rate proportional to the star

---

[19] The analysis of Ménard, Kilbinger & Scranton (2010b) assumed the slightly lower value $R_V = 3.9 \pm 2.6$.

[20] For a detailed list of references see Sec. 2 of Höflich et al. (2010).

formation rate (~ 0.5 Gyr timescale), while the latter group consists of intrinsically dimmer fast decliners, which take several Gyr to explode and come from much older populations with a rate proportional to the mass of the host galaxy (Sullivan et al. 2006). Since star formation rate increases over the redshift ranges in which SNe Ia occur, the number of "prompt" SNe Ia will increase with redshift, and therefore the mean luminosity of the population should increase with redshift (Howell et al. 2007).

It is quite possible that it is intrinsic effects related to the differences between the prompt and delayed events which are not fully accounted for with the current light curve fitters. However, light curve corrections can reverse the trends in the underlying population if the fitter only assumes a single class of standardizable object, when there is actually more than one. Recent studies by Sullivan et al. (2010) and Lampeitl et al. (2010) both find a statistically significant correlation between SN Ia luminosity and host galaxy type. In particular, more passively evolving galaxies tend to host SNe Ia which, *after light curve correction* are of order 0.1 mag brighter than those in galaxies with high specific star formation rates. The passively evolving galaxies are generally more massive, and so there is a related correlation, which has also been observed in earlier work with smaller nearby samples (Kelly et al. 2010). Sullivan et al. (2010) studied SNLS data using the SiFTO light curve fitter, which uses a similar methodology to SALT. They found that events of the same light-curve shape and colour were on average 0.08 mag brighter, at 4σ confidence, for the the passively evolving subclass of SNe Ia. The passively evolving subclass also favoured smaller values of the SALT-like parameter β than those in galaxies with significant star formation, at the 2.7σ confidence level. Very similar results were obtained by Lampeitl et al. (2010) using SNLS data and both the SALT-II and MLCS2k2 fitters. For MLCS2k2, the favoured value of the parameter R_V is found to be different between the two subclasses, with values $R_V \sim 1$ favoured by the passively evolving subclass and $R_V \sim 2$ by the the star-forming hosts.

Both Sullivan et al. (2010) and Lampeitl et al. (2010) recommend correcting light curves based on two sets of SN Ia templates, depending on galaxy types. Since the effective Ω_{m0} parameter of the TS cosmology is more sensitive to the differences between different light curve fitters, it would be extremely interesting to test what effect this would have.

6 CONCLUSION

In conclusion, we find that the principal criticism of the TS cosmology made by Kwan et al. (2009) does not hold up when the issues surrounding the systematics of SN Ia data reduction are thoroughly investigated. In particular, the unreasonably small bestfit values of Ω_{m0} (or equivalently the unreasonably high bestfit values of the void fraction, f_{v0}) for the full Union and Constitution datasets are an artifact of failing to exclude SNe Ia below the scale of statistical homogeneity from the analysis. Such a cut must be made for the purpose of consistency with the TS model, given that an apparent Hubble bubble with certain characteristics will be found below the SHS. The main issue is not the size of the

datasets, as Kwan et al. (2009) claimed, but the systematics of the data reduction methods.

We have shown that when suitable cuts are made then the SALT/SALT-II fitters, as currently implemented, provide Bayesian evidence to favour the spatially flat ΛCDM model over the TS model. However, by contrast the MLCS2k2 similarly provide Bayesian evidence that favours the TS model over the spatially flat ΛCDM model. Basically, both models are a very good fit and it is the light curve fitting systematics that underlie the few percent level differences which have to be sorted out to distinguish the two cosmologies.

As yet these systematics are not fully understood, and involve many subtleties. For example, the value of $\Omega_{m0} = 0.42 \pm 0.10$ obtained for the TS model with the SHS-cut SDSS-II sample is twice the corresponding value for the SHS-cut MLCS17 sample, $\Omega_{m0} = 0.19^{+0.14}_{-0.17}$, despite their similar R_V values. It is clear that the differences do not involve a single parameter alone. Nonetheless, given that an apparent Hubble bubble below the scale of statistical homogeneity is a feature of the TS scenario, the differences between SHS cuts applied to the MLCS17 and MLCS31 samples suggest consistency for the TS scenario if galaxies which host "normal" SNe Ia events have a reddening law with R_V value close to the Milky way value, $R_V \simeq 3.1$, at least *at low redshifts*. Distinguishing "normal" SNe Ia from other events may be further complicated by

• the existence of a subclass of events with nonstandard dust, possibly related to circumstellar dust, as evidenced by the study of Wang et al. (2009);

• the existence of an intrinsic colour variation, uncorrelated with decline rate, which distinguishes "normal" SNe Ia in passively evolving galaxies from those in galaxies with significant star formation, as evidenced by many studies including the recent studies of Sullivan et al. (2010) and Lampeitl et al. (2010).

In our opinion systematic questions should ideally be resolved by detailed studies which attempt to understand the astrophysics involved with as few cosmological assumptions as possible, rather than purely empirical correlations based on homogeneous cosmologies. For example, in trying to sort out systematics at the percent level the current approach is often to test how variation of empirical parameters affects Hubble residuals, using a standard ΛCDM model or a homogeneous dark energy cosmology with fixed equation of state parameter, w. However, such a parameterisation has no meaning for the TS cosmology, as was demonstrated in Fig. 3 of Wiltshire (2009), where the equivalent $w(z)$ determined from a perfectly smooth luminosity distance relation was found to be ill–defined at $z \sim 1.7$.

Furthermore, from the viewpoint of the TS model distinctions based on Hubble residuals should *not be used below the scale of statistical homogeneity*, $z \lesssim 0.033$, since a natural variance in the Hubble flow is to be expected below this scale. The only scales within which Hubble residuals would be a safe determinant of empirical correlations would be over those scales beyond the SHS over which an effective linear global average Hubble law pertains, e.g., on scales $0.033 \lesssim z \lesssim 0.1$. Beyond such a scale any Hubble residuals, whether based on the ΛCDM model, the TS model or any other model, are cosmology-dependent.

For a simple two model comparison it would be important to fully re-perform the MLCS reduction, including cuts based on extinction priors, using the TS model from the outset. Likewise, the changes to Hubble residuals with different classes of SN Ia light curves for passively evolving galaxies, as opposed to star-forming galaxies, should be investigated.

Given that the issue of dust extinction and reddening laws is so entangled with the question of intrinsic colour variations, we really require many independent studies, such as those of Finkelman et al. (2008, 2010), which examine reddening laws in other galaxies without any reference to SNe Ia.

Cosmology is a unique science, in the sense that its most basic quantity – distance – can only be determined by assuming a cosmological model when interpreting measurements such as spectra, apparent magnitudes and angles on the sky. We have to be careful to recognize how the cosmological models we assume affect our approach to data reduction. The TS model is a well-motivated alternative to the standard ΛCDM model with some very different properties to homogeneous cosmologies and cannot be parameterised by a well-defined dark energy equation of state parameter, even though the luminosity distance is close to that of FLRW models. The differences between the two models are at the same level as the current systematic uncertainties in SN Ia data reduction which need to be disentangled. We therefore hope that the TS model might be used alongside the standard cosmology as a test bed for trying to determine which systematic effects are truly astrophysical, and which might have an origin in cosmological assumptions.

REFERENCES

Amanullah R. *et al.*, 2010, ApJ **716**, 712.
Bennett C.L. *et al.* 2003, ApJ Suppl. **148**, 1.
Blondin S. *et al.*, 2009, ApJ **693**, 207.
Buchert T., 2000, Gen. Relativ. Grav. **32**, 105.
Buchert T., 2008, Gen. Relativ. Grav. **40**, 467.
Buchert T., Carfora M., 2002, Class. Quantum Grav. **19**, 6109.
Buchert T., Carfora M., 2003, Phys. Rev. Lett. **90**, 031101.
Buchert T., Larena J., Alimi J. M., 2006, Class. Quantum Grav. **23**, 6379.
Cardelli J. A., Clayton G. C., Mathis J. S., 1989, ApJ **345**, 245.
Cole S. *et al.*2005, MNRAS **362**, 505.
Conley A., Carlberg R. G., Guy J., Howell D. A., Jha S., Riess A. G., Sullivan M., 2007, ApJ **664**, L13.
Courbin F. *et al.*, 2010, arXiv:1009.1473.
Eisenstein, D.J. *et al.* 2005, ApJ **633**, 560.

Ellis G. F. R., 1984, in Bertotti B., de Felice F., Pascolini A. (eds), *General Relativity and Gravitation*, (Reidel, Dordrecht) pp. 215–288.
Ellis G. F. R., Stoeger W., 1987, Class. Quantum Grav. **4**, 1697.
Finkelman I. *et al.*, 2008, MNRAS **390**, 969.
Finkelman I. *et al.*, 2010, arXiv:1008.5149.
Freedman W. L. *et al.*, 2001, ApJ **553**, 47.
Folatelli G. *et al.*, 2010, AJ **139**, 120.
Freedman W. L. *et al.*, 2009, ApJ **704**, 1036.
Goobar A., 2008, ApJ **686**, L103.
Guy J., Astier P., Nobili S., Regnault N., Pain R., 2005, Astron. Astrophys. **443**, 781.
Guy J. *et al.*, 2007, Astron. Astrophys. **466**, 11.
Hamuy M., Phillips M. M., Maza J., Suntzeff N. B., Schommer R. A., Aviles R., 1995, AJ **109**, 1.
Hicken M. *et al.*, 2009, ApJ **700**, 1097.
Höflich P. *et al.*, 2010, ApJ **710**, 444.
Hogg D. W., Eisenstein D. J., Blanton M. R., Bahcall N. A., Brinkmann J., Gunn J. E., Schneider D. P., 2005, ApJ **624**, 54.
Howell D. A., Sullivan M., Conley A. J., Carlberg R., 2007, ApJ **667**, L37.
Hoyle F., Vogeley M. S., 2002, ApJ **566**, 641.
Hoyle F., Vogeley M. S., 2004, ApJ **607**, 751.
Jha S., Riess A. G., Kirshner R. P., 2007, ApJ **659**, 122.
Kelly P. L., Hicken M., Burke D. L., Mandel K. S., Kirshner R. P., 2010, ApJ **715**, 743.
Kessler R. *et al.*, 2009, ApJ Suppl. **185**, 32.
Komatsu E. *et al.*, 2010, arXiv:1001.4538.
Kwan J., Francis M. J., Lewis G. F., 2009, MNRAS **399**, L6.
Kowalski M. *et al.*, 2008, ApJ **686**, 749.
Lampeitl H. *et al.*, 2010, ApJ **722**, 566.
Leibundgut B., 2008, Gen. Relativ. Grav. **40**, 221.
Leith B. M., Ng S. C. C., Wiltshire D. L., 2008, ApJ **672**, L91.
Li N., Schwarz D. J., 2008, Phys. Rev. **D 78**, 083531.
Larena J., Alimi J. M., Buchert T., Kunz M., Corasaniti P. S., 2009, Phys. Rev. **D 79**, 083011.
Mattsson M. & Mattsson T., 2010, JCAP 10, 021.
Mattsson T., 2009, Gen. Relativ. Grav. **42**, 567.
Ménard B., Scranton R., Fukugita M., Richards G. 2010, MNRAS **405**, 1025.
Ménard B., Kilbinger M., Scranton R., 2010, MNRAS **406**, 1815.
Oguri M., 2007, ApJ **660**, 1.
Patat F. *et al.*, 2007, Science **317,** 924.
Patat F., Baade D., Hoeflich P., Maund J. R., Wang L., Wheeler J. C., 2009, Astron. Astrophys. **508**, 229.
Perlmutter S. *et al.*, 1999, ApJ **517**, 565.
Räsänen S., 2006, JCAP 11, 003.
Räsänen S., 2008, JCAP 04, 026.
Reese E. D., Kawahara H., Kitayama T., Ota N., Sasaki S. & Suto Y., 2010, ApJ **721**, 653.
Riess A. G., Press W. H., Kirshner R. P., 1995, ApJ **438**, L17.
Riess A. G. *et al.*, 1998, AJ **116**, 1009.
Riess A. G. *et al.*, 2005, ApJ **627**, 579.
Riess A. G. *et al.*, 2007, ApJ **659**, 98.
Riess A. G. *et al.*, 2009, ApJ **699**, 539.

Sandage A., Tammann G.A., Saha A., Reindl B., Macchetto F.D., Panagia N., 2006, ApJ **653**, 843.

Scannapieco E., Bildsten L., 2006, ApJ **629**, L85.

Sinclair B., Davis T. M., Haugbølle T., 2010, ApJ **718**, 1445.

Sollerman J. *et al.*, 2009, ApJ **703**, 1374.

Spergel D.N. *et al.* 2007, ApJ Suppl. **170**, 377.

Sullivan M. *et al.*, 2006, ApJ **648**, 868.

Sullivan M. *et al.*, 2010, MNRAS **406**, 782.

Sylos Labini F., Vasilyev N. L., Baryshev Y. V., López-Corredoira M., 2009, Astron. Astrophys. **505**, 981.

Tikhonov A. V., Karachentsev I. D., 2006, ApJ **653**, 969.

Trotta R., 2008, Contemp. Phys. **49**, 71.

Wang X., Li W., Filippenko A. V., 2008, ApJ **675**, 626.

Wang X., Li W., Filippenko A. V., Foley R. J., Smith N., Wang L., 2008, ApJ **677**, 1060.

Wang X. *et al.*, 2009, ApJ **699**, L139.

Wiegand A., Buchert T., 2010, Phys. Rev. **D 82**, 023523.

Wiltshire D. L., 2007a, New J. Phys. **9**, 377.

Wiltshire D. L., 2007b, Phys. Rev. Lett. **99**, 251101.

Wiltshire D. L., 2008, Phys. Rev. **D 78**, 084032.

Wiltshire D. L., 2009, Phys. Rev. **D 80**, 123512.

Wood–Vasey W. M. *et al.*, 2007, ApJ **666**, 694.

Zehavi I., Riess A. G., Kirshner R. P., Dekel A., 1998, ApJ **503**, 483.